NTNU
Norwegian University of
Science and Technology

Quantitative Refraction Traveltime Analysis of 3D Seismic Acquired After an Underground Blowout in the Central North Sea

Bjarte Foseide

Petroleum Geoscience and Engineering
Submission date: June 2017
Supervisor: Martin Landrø, IGP

Norwegian University of Science and Technology
Department of Geoscience and Petroleum

Abstract

A quantitative refraction traveltime analysis was performed in this thesis. Refraction seismic can be used for monitoring in shallow parts of the subsurface where the contribution from conventional reflection data is inadequate. As the refractions move primarily in the horizontal direction, opposed to the more vertical travel-path of the reflections, they can detect smaller variations below interfaces. One obvious limitation regarding refractions is the requirement of a positive velocity contrast, another is that the deeper events will be influenced by shallower refractions.

An underground blowout in well 2/4-14 in 1989 led to gas migrating into several shallow sand layers, and it was investigated if the traveltime of refracted events could be used to identify and map the horizontal extent of gas accumulations in these layers.

A processing and analysis workflow was successfully established and several refracted events were mapped in a six by six km^2 area around the blowout well. The raw seismic data was processed with two different Ormsby bandpass filters, where the lowest frequency filter with limits (2-5-15-20) Hz illustrated best the potential of this method. Numerous refractions at various offsets were initially analysed, but the focus of this thesis is on the most promising and interesting refractions. Results presented are for refractions mapped at two different offsets, 1075 m and 3563 m.

A refraction traveltime anomaly at an estimated depth of 154-176 m was identified and mapped. The refraction traveltime matched the results of a refraction time-shift analysis along a 2D line for data acquired prior to, and 20 months after the blowout. With this, it was interpreted that the shallow refraction traveltime anomaly is caused by gas from the blowout. It is believed that this gas migrated into a tunnel valley and 3 years after the blowout, most of the gas appears to have migrated 800 m SE of the blowout well.

Refraction traveltimes for four refracted events were successfully mapped at a very high offset. They all showed significant anomalies around the blowout well. Two of the refractions are believed to correspond to amplitude anomalies visible in reflection seismic and the other two possibly shows gas anomalies not visible in the reflection data. The fact that the refraction traveltime anomalies also are more well defined illustrates some advantages with using refractions to map the shallow subsurface.

The results in this thesis demonstrate a way to use refraction traveltimes as a method of mapping the shallow subsurface. Despite the limitations, gas in several sand layers from the underground blowout were successfully identified and mapped.

Sammendrag

En kvantitativ refraksjon gangtidsanalyse ble utført i denne masteroppgaven. Refraksjonsseismikk kan brukes til overvåkning i grunne deler av undergrunnen hvor bidraget fra konvensjonelle refleksjonsdata er utilstrekkelig. Da refrakterte bølger hovedsakelig beveger seg i horisontal retning, i motsetning til den mer vertikale gangveien til refleksjonene, kan de oppdage mindre variasjoner under grenseflater. En åpenbar begrensning for refraksjoner er avhengigheten av positiv hastighetskontrast, en annen er at de dypere refraksjonene vil bli påvirket av de grunnere refraksjonene.

En underjordisk gassutblåsning i brønn 2/4-14 i 1989 førte til at gass migrerte inn i flere grunne sandlag, her har det har blitt undersøkt om gangtiden til refrakterte bølger kan brukes til å identifisere og horisontalt kartlegge gassakkumuleringer i disse lagene.

En fremgangsmåte for prosessering og analyse av dataene ble satt opp, og flere refrakterte bølger ble kartlagt i et seks ganger seks km^2 stort område rundt utblåsningsbrønnen. De rå seismiske dataene ble prosessert med to forskjellige Ormsby bandpass filter, hvor det laveste frekvensfilteret med grensene (2-5-15-20) Hz viste best potensialet for denne metoden. Flere refraksjoner ved ulike offset ble i første omgang analysert, men fokuset i denne oppgaven ble på de mest lovende og interessante refraksjonene. Resultatene presentert her er for refraksjoner kartlagt ved to forskjellige offset, 1075 m og 3563 m.

Et avvik i gangtiden til en refraksjon fra en estimert dybde på 154-176 m ble identifisert og kartlagt. Gangtiden til refraksjonen matchet resultatene til en refraksjons tids-skift analyse langs en 2D-linje for data samlet før, og 20 måneder etter utblåsningen. Med dette ble det tolket at det grunne avviket i refraksjons gangtid skyldtes gass fra gassutblåsningen. Det antas at denne gassen migrerte inn i en tunneldal, og 3 år etter gassutblåsningen virker det som en stor del av gassen har migrert 800 m sør-øst for utblåsningsbrønnen.

Gangtider for fire refraksjoner ble vellykket kartlagt på svært høyt offset. De viste alle signifikante anomalier rundt utblåsningsbrønnen. To av refraksjonene antas å korrespondere med amplitude-anomalier synlige i refleksjonsseismikken, og de andre to viser muligens gassanomalier som ikke er synlige i refleksjonsdataene. Det faktum at refraksjons-anomaliene også er noe mer veldefinerte, illustrerer noen av fordelene ved å bruke refraksjoner for å kartlegge den grunne undergrunnen.

Resultatene i denne avhandlingen illustrerer en måte å bruke refraksjons gangtider som en metode for kartlegging av den grunne undergrunnen. Til tross for begrensningene ble gass i flere sandlag fra en underjordisk utblåsing vellykket identifisert og kartlagt.

Preface

This master's thesis was written by Bjarte Foseide during the spring of 2017. It is the final part of a 5-year study program leading to an M.Sc. in Petroleum Geosciences at the Norwegian University of Science and Technology (NTNU).

First, I would like to thank my supervisor Martin Landrø for his guidance, scientific advice and useful discussions through this process. The work in this thesis sparked from an idea he provided.

I would also like to thank Elisabeth Grindstad whom I collaborated with during the initial part of the thesis. Understanding the provided data and setting up the initial processing steps went a lot faster when we worked together.

Last, I want to thank my family, my wife and son, for their support during my studies and for just making my days brighter.

Bjarte Foseide,
Trondheim, June 2017

Table of Contents

List of Tables

List of Figures

Abbreviations

CDP	Common Depth Point
km	kilometre
m	metre
ms	milliseconds
RMS	Root Mean Square
std	standard deviation

Chapter 1

Introduction

1.1 Background and motivation

Refraction seismic methods utilize waves that have been refracted at the critical angle, these waves are commonly known as head waves or simply refractions (Sheriff and Geldart, 1995). The main difference between reflection and refraction methods is the difference in offset needed, where the offset for refraction methods is large relative to the depth of investigation. That means that the travel path for the refracted methods are dominantly horizontal and for the reflection methods it is dominantly vertical. The fact that the travel path in refraction methods is dominantly horizontal results in incoming waves that can be heavily affected by thinner layers. These layers might not be observable with reflection methods, at least at very shallow depths. Refraction seismic can then be used for monitoring in shallow parts of the subsurface where the contribution from conventional reflection data is inadequate.

Landrø et al. (2004) introduced time-lapse refraction seismic as a method to estimate reservoir velocity changes. They used RMS amplitude analysis versus offset to measure the shift in peak amplitude, caused by a change in critical offset, between a base and monitor survey. With this change in peak RMS amplitude offsets it is possible to estimate the velocity change in the layer in question.

By measuring the time-shift of first arrival head waves from a refracting layer below a reservoir Hansteen et al. (2010) found plausible one-way timelapse time-shifts in the reservoir in the order of 2 ms. The large scale time-shifts observed may be a result of variation in fluid pressures, but smaller local variations was interpreted as changes in gas saturation.

Zadeh and Landrø (2011) demonstrates the potential of refraction seismic as a complementary 4D analysis technique. With a standard windowed cross-correlation technique, they found consistent time-shifts of up to 4 ms when comparing a base survey acquired before a blowout with a monitor survey taken 20 months after the blowout. The time shifts are interpreted to be caused by shallow gas after the underground blowout.

In January 1989 Saga Petroleum drilled an exploration well (2/4-14) in the southern part of the North Sea, they experienced a kick which resulted in an underground blowout. The seismic reflection data show clear indications where most of the gas has migrated. However, the gas may have migrated into very shallow sand layers and possibly far from the well if pathways with high permeability are present. Halvorsen (2012) map tunnel valleys in the area around the blowout well and evaluates that the possibility of gas migration within the tunnel valleys is believed to be conspicuous.

Shallow seismic are usually heavily influenced by seabed multiples and generally low resolution, as a result of this the possibility of interpreting reflectors and doing an analysis of reflection data is limited. On the other hand, refraction seismic does not suffer from these limitations at shallow depths and can then be used for analysis. By shallow seismic depths less 500 m is meant here.

Mapping shallow gas is of great importance. In general it is of interest how hydrocarbons migrate and in this case study with the underground blowout, this is also important as it needs to be verified that there is no gas leakage to the sea. Shallow gas might be regarded as a geohazard, this can pose a risk to crew, installations, and the environment. How gas migrates in the shallow subsurface is also important to understand when it comes to CO_2 and other environmental gasses storage scenarios.

The idea is that potential shallow gas anomalies can be mapped using refraction seismic methods.

1.2 Goal and method

The study of time-lapse time-shifts for a refracted event by Zadeh and Landrø (2011) formed the basis for this thesis. In this thesis, traveltime to refracted events is used to identify and map shallow anomalies caused by an underground hydrocarbon flow. The data provided for this

thesis is not 4D, but 3D. It is believed that the possible gas anomalies influence the refraction traveltimes enough so the horizontal extent can be mapped.

The following list states some of the major steps done in this thesis.

- Set up a processing and analysis workflow to be able to map refraction traveltimes around the blowout well.
- Map the extent of the shallow gas anomaly found by Zadeh and Landrø (2011).
- See if there are any connections between the refraction traveltimes and mapped tunnel valleys in the area.
- See if it is possible to map deeper refractions, possible ones influenced by the gas accumulation at 490 m caused by the blowout.
- Do synthetic seismic modeling to estimate depths of the possible gas anomalies presented.

Because of lack of time the last point was not achieved. As a result of this, there are not estimations of depths for all the mapped refractions.

1.3 Outline

This thesis is divided into several chapters. First, background information about the blowout and the geology in the area are presented in Chapter 2. Then, Chapter 3 moves on to describe some of the theory behind refraction seismic and the software used. In addition, a section in this chapter describes theory about cross-sections through a circular object that is useful for understanding the final results. The available data, that consists of both raw and processed 3D data and some well data, is given in Chapter 4. In Chapter 5 the methods used to generate the results are stated. The method consists of both processing in ProMAX and analysis in MatLab. The results are presented in Chapter 6. This chapter consists of three sections where the first two present results based on two different processing sequences respectively and the third present a comparison between the results and tunnel valleys in the area. There are uncertainties regarding the results in this thesis, together with the results they are discussed in Chapter 7. This chapter also presents some possible interpretations of the results. In the end, Chapter 8 summarizes the work, draws conclusions and provide with propositions for further work.

Chapter 2

Geology

2.1 Study area setting

The study area is located around well 2/4-14 in the southern part of the North Sea. For this thesis, only the uppermost part of the subsurface is of interest, i.e. shallower than 500 metres. In the North Sea the shallower parts are considered to be of the Nordland group. The Nordland group is of middle Miocene to recent age and stretches from the southern North Sea up to the western Barents Sea. (NORLEX, n.d.)

In the North Sea, the Nordland Group mainly consists of claystone deposited in a marine environment. In the Viking Graben area, north of the study area, Utsira Formation can be found at the bottom of the Nordland Group. Due to its high porosity and permeability sand, this saline aquifer is at the Sleipner field used as a CO_2 storage site (Arts et al. (2008), Chadwick et al. (2004)). The upper parts of the group consist of unconsolidated clay and sand with some occasionally ice rafted debris. Glacial deposits increase in the uppermost part of the group. (NORLEX, n.d.)

2.1.1 Gas blowout, well 2/4-14

In October 1988 Saga Petroleum ASA started the drilling of exploration well 2/4-14, with the primary objective to assess the hydrocarbon potential in a rotated fault block on the Steinbit terrace. The target was expected to be a late Jurassic sandstone (NPD, n.d.). In January 1889 at depth 4734 m the well kicked. After several attempts to regain control of the well without success, the well was shut. This resulted in an underground blowout, i.e. when fluid flow

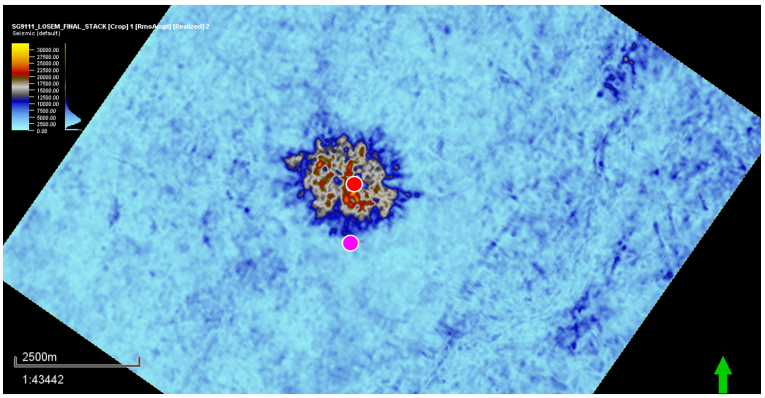

Figure 2.1: RMS amplitude at 524 ms for a 10 ms timewindow from a 3D seismic cube. The large anomaly visible around well 2/4-14 (red circle) is approximately 2 km in diameter. The magenta circle marks the location of well 2/4-15 almost 1.2 km south of the blowout well.

uncontrollably from one reservoir in to the wellbore, along the wellbore, and in to another reservoir (Schlumberger, 2017b). After several attempts to kill the well failed, the rig was moved and drilling of a relief well started. Well 2/4-15 approximately 1,2 km South of the blowout well. The underground blowout was stopped and well 2/4-14 killed on 13. December 1989 (Landrø, 2011).

The hydrocarbons that migrated into shallow sand layers and are clearly visible on the seismic. Figure 2.1 show the Root Mean Squared (RMS) amplitude for a 10 ms time window at 524 ms depth, there is a large amplitude anomaly that extends approximately 1 km in radial distance from well 2/4-14. This is caused by gas from the blowout.

2.2 North Sea tunnel valleys

Tunnel valleys are carved in to deposited sediments or bedrock during glaciations. They are frequently sinuous and usually form anastomosing networks, but can also form individual straight valleys. The sedimentary infill varies but is characteristically dominated by sediment gravity flow facies and thick glaciofluvial sands. (Cofaigh, 1996)

Shallow tunnel valleys within block 2/4 can act as migration paths for leaked gas in the area (Halvorsen, 2012).

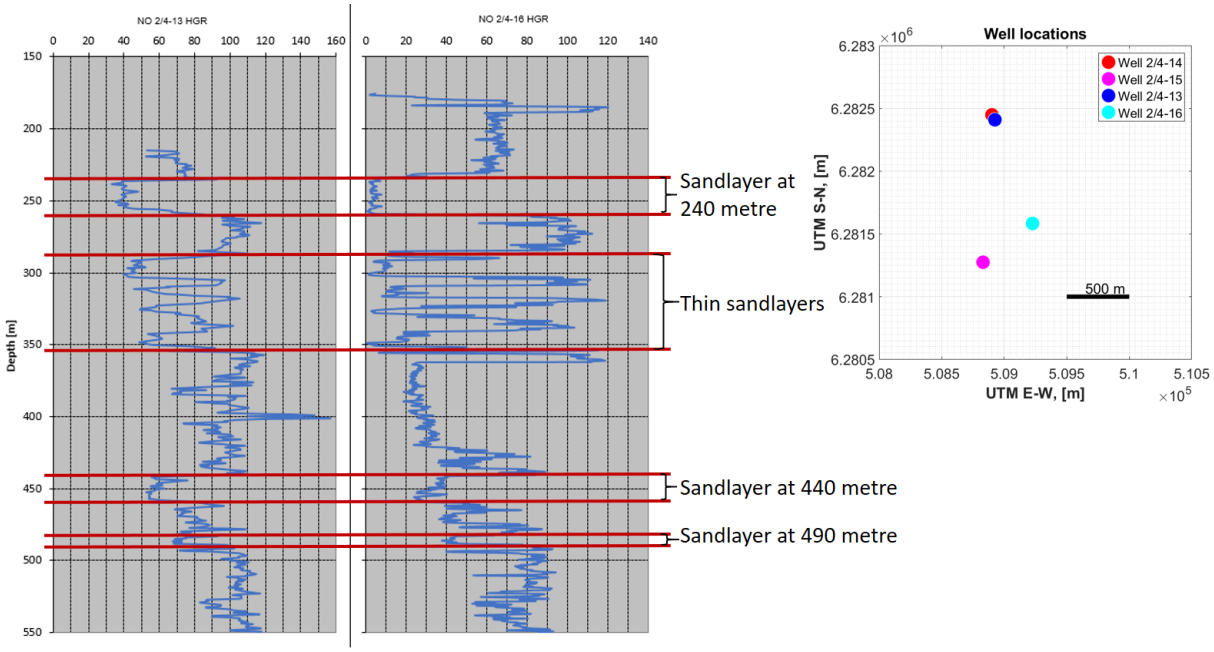

Figure 2.2: Gamma-ray logs from wells 13 and 16 at depths <550 m. The log to the left from 2/4-13 starts at ∼210 m and the log from 2/4-16 starts at ∼170 m. Locations of the different wells 13, 14, 15 and 16 are shown to the top right, with locations in UTM coordinates.

2.3 Shallow sands and gas

At shallow depths there are very limited available well logs in this area. Figure 2.2 shows a comparison between gamma-ray logs taken in two wells in close vicinity of the blowout well. 2/4-13 and 2/4-16 are situated with a horizontal distance of 880 metres between them, well locations are also shown in the figure. The low gamma-ray readings are interpreted as shallow sand layers. As highlighted by the red lines on the logs there is good correlation between the gamma-ray logs indicating that the interpreted sand layers are laterally continuous.

Most of the hydrocarbons that escaped into shallow sands are believed to have migrated into a sand layer at 840 m depth, it is estimated that ten months after the blowout the hydrocarbon anomaly at his depth extended over a 15 km^2 area (Landrø, 2011). Gas also migrated into the sand layers at approximately 440 and 490 metres, mainly into the 490-m sand. The large amplitude anomaly visible in figure 2.1 corresponds to the 490 m sand layer. Saga Petroleum also identified sand layers at depths 523 m, 562 m and 605 m in addition to the sand layers at 490 and 840 m depth that all can serve as hosts for the blowout gas.

Chapter 3

Theory

3.1 Refraction seismic

A two-layered, isotropic homogeneous model is illustrated in figure 3.1, assuming a plane wave propagating in this model the equation for refraction travel time at offset larger than critical offset can be derived.

From geometry in figure 3.1 the refracted traveltime, t, is given as

$$t = \frac{L}{V_2} + \frac{2d}{V_1}. \tag{3.1}$$

Here 2d is the distance the wave travels in the first layer and L is the distance the refracted wave travels in the second layer. V_1 and V_2 are the P-wave velocities for the layers, respectively. Replacing L with offset, X, and critical offset, X_c, and using trigonometric identities we get

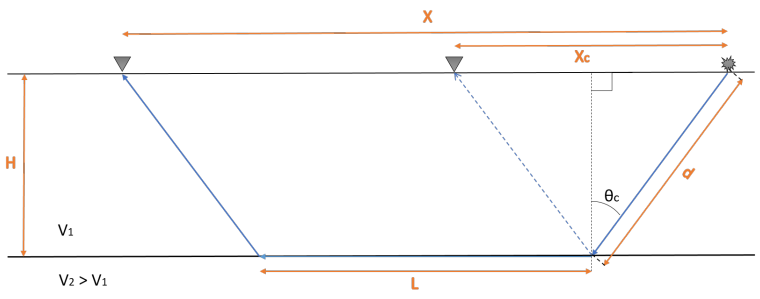

Figure 3.1: Schematic illustration of refraction travel path. The interface for the velocity increase from V_1 to V_2 is located at depth H.

$$t = \frac{X - X_c}{V_2} + \frac{2H}{V_1 cos(\theta_c)}, \qquad X \geq X_c, \tag{3.2}$$

$$t = \frac{X}{V_2} - \frac{2Htan(\theta_c)}{V_2} + \frac{2H}{V_1 cos(\theta_c)}, \qquad X \geq X_c \tag{3.3}$$

and

$$t = \frac{X}{V_2} + \frac{2H}{V_1}\left(\frac{1}{cos(\theta_c)} - \frac{V_1 tan(\theta_c)}{V_2}\right), \qquad X \geq X_c. \tag{3.4}$$

H is the depth of the interface for the velocity increase from V_1 to V_2 and θ_c is the critical angle at this interface. Substituting in Snell's law at critical angle, $sin(\theta_c) = \frac{V_1}{V_2}$, we get

$$t = \frac{X}{V_2} + \frac{2H}{V_1}\left(\frac{1}{cos(\theta_c)} - sin(\theta_c)tan(\theta_c)\right), \qquad X \geq X_c. \tag{3.5}$$

Simplifying the equation gives

$$t = \frac{X}{V_2} + \frac{2H}{V_1}\left(\frac{1 - sin^2(\theta_c)}{cos(\theta_c)}\right), \qquad X \geq X_c. \tag{3.6}$$

Further simplifying with the Pythagorean trigonometric identity, $sin^2(\theta) + cos^2(\theta) = 1$, gives

$$t = \frac{X}{V_2} + \frac{2H}{V_1}\left(\frac{1 - sin^2(\theta_c)}{\sqrt{1 - sin^2(\theta_c)}}\right), \qquad X \geq X_c. \tag{3.7}$$

Simplifying and substituting in Snell's law here we get

$$t = \frac{X}{V_2} + \frac{2H}{V_1}\sqrt{1 - \left(\frac{V_1}{V_2}\right)^2}, \qquad X \geq X_c. \tag{3.8}$$

Here t is an equation in the form of, y=ax+b, where $\frac{1}{V_2}$ is the slope and the second part is the intercept with the y-axis.

3.2 Refraction time-shifts

Assuming a small velocity change below the interface and an anomaly that appears infinite, i.e. V_2 below the interface is changed by ΔV_2, the refraction time-shift can be estimated. Depth to interface H, velocity above interface V_1 and offset X are kept constant. The time-shift can be

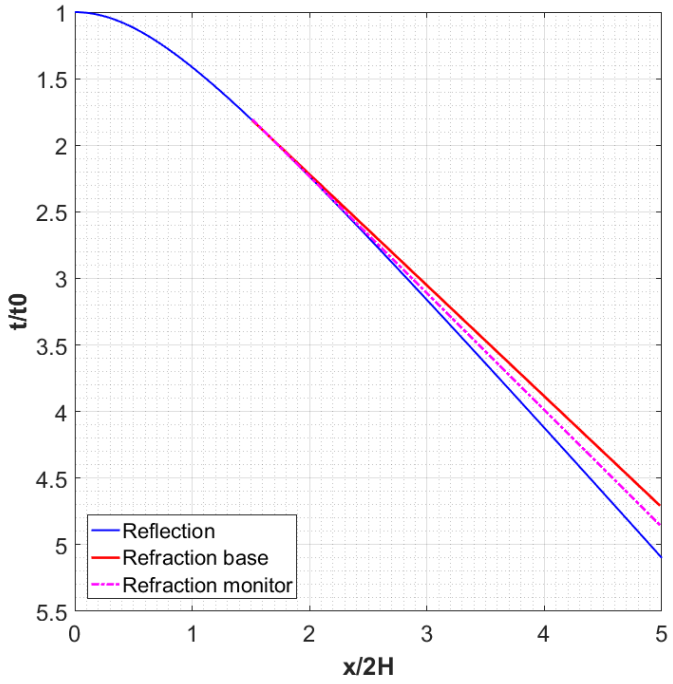

Figure 3.2: Reflection and refraction traveltime (relative to zero offset traveltime, t_0) versus offset (relative to depth, 2H) for a 5% timelapse velocity decrease in V_2. The difference between refraction base (red) and monitor (dashed magenta) starts at critical offset and increase linearly with offset. Figure was inspired by Zadeh and Landrø (2011).

approximated by taking the first derivative of equation 3.8, which gives

$$\Delta t \approx \left(\frac{2HV_1}{\sqrt{V_2^2 - V_1^2}} - X \right) \frac{\Delta V_2}{V_2^2}, \qquad X \geq X_c. \tag{3.9}$$

This equation shows that the relative time-shift is linearly increasing with offset. Figure 3.2 show an example of a base and monitor scenario where the velocity below the interface is decreased by 5%. This figure shows that small velocity differences clearly affects the traveltime of the refraction.

Note that this is a 1D example and would be equivalent to an anomaly with infinite lateral extension in 2D. For a 2D anomaly with limited extension E, as shown in figure 3.3, the refraction time-shift depends on the offset.

Following the deriving in Zadeh and Landrø (2011) two different monitor traveltime scenarios can happen,

$$t' = \frac{\sqrt{X_c^2 + 4H^2}}{V_1} + \frac{E}{V_2'}, \qquad X \geq X_c + E, \tag{3.10}$$

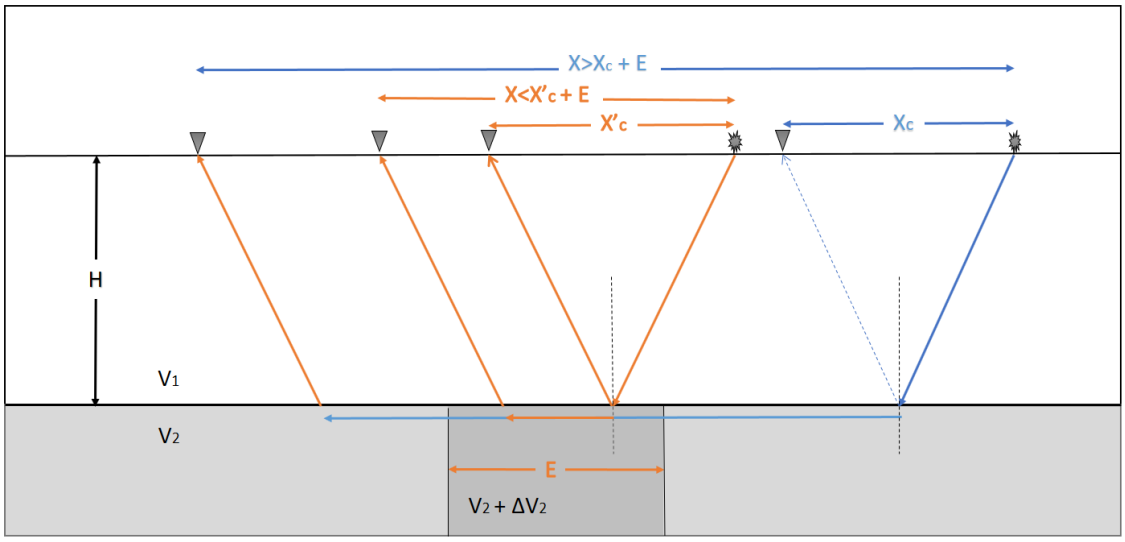

Figure 3.3: Schematic illustration of an anomaly with limited extension E with an velocity $V_2 + \Delta V_2$ in a layer with velocity V_2. The figure is inspired by a figure in Zadeh and Landrø (2011).

and

$$t' = \frac{\sqrt{X_c'^2 + 4H^2}}{V_1} + \frac{X - X_c'}{V_2'}, \qquad X_c < X < X_c + E, \tag{3.11}$$

where X_c is the critical offset and E is the extent of the anomaly. V_2' is the weighted average velocity in layer two and X_c' is the critical offset within the anomaly. Taking the first derivative, assuming small velocity change, the refraction time-shift can be estimated as

$$\Delta t \approx -E\frac{\Delta V_2}{V_2^2}, \qquad X \geq X_c + E, \tag{3.12}$$

and

$$\Delta t = -\left(X - \frac{2HV_1}{\sqrt{V_2^2 - V_1^2}}\right)\frac{\Delta V_2}{V_2^2}, \qquad X_c < X < X_c + E. \tag{3.13}$$

As seen in these equations, 3.12 and 3.13, the time-shift start at critical offset and increase linearly until max time-shift is achieved for offsets equal to or larger than $(X_c + E)$. For offsets smaller than critical offset the time-shift is zero.

3.3 Circle geometry

The equation for a circle with centre in the origin can be written as

$$r^2 = x^2 + y^2. \tag{3.14}$$

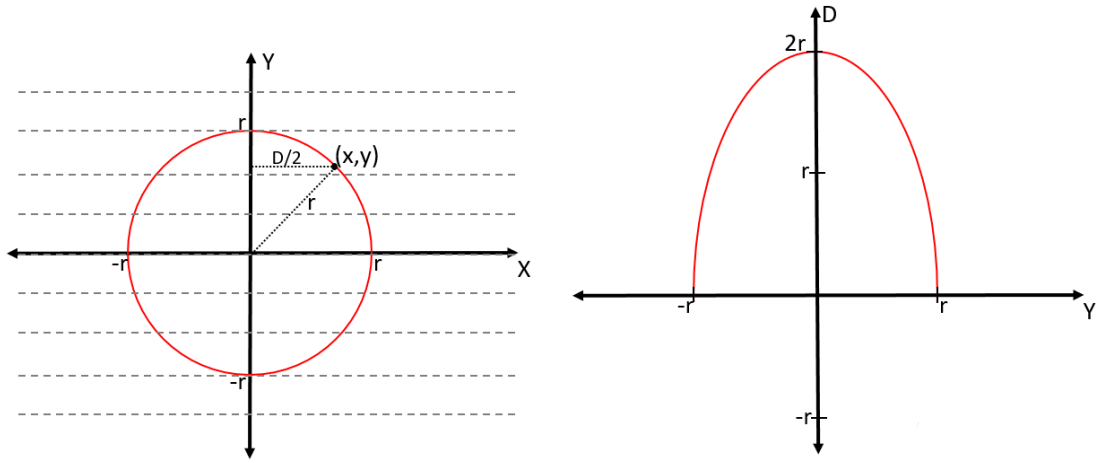

Figure 3.4: The figure to the left shows a circle with centre in the origin with radius r. The dotted lines are parallel to X-axis. The curve to the right show the length, D, of the cross-section through the circle observed when cut parallel to the X-axis.

Here r is the radius of the circle and (x, y) is a point on the circle edge. The left illustration in figure 3.4 shows a circle with radius r with centre at the origin.

The length, D, of the circle seen when sliced along the dotted lines parallel to the X-axis can be written as

$$D = 2\sqrt{r^2 - y^2}. \tag{3.15}$$

The length D is maxed at 2r when y=0 and decreases with the rate of $-\frac{2y}{\sqrt{r^2-y^2}}$ to zero when the value of y goes to r. This length of the circle observed when cut parallel to the X-axis is shown in figure 3.4 to the right.

In other words, a circular velocity anomaly that is mapped by averaging the velocity along parallel lines of the X-axis will experience that when the distance from the anomaly's origin increase towards r the amount of the anomaly observed along the line decrease rapidly.

3.4 Software

The main programs used in thesis and their primary usage are listed here.

ProMAX is an extensive seismic processing system for large volume marine or land surveys, 2D or 3D pre- and post-stack data. This was used to process raw seismic data.

MATLAB, MATrix LABoratory, is a high-level programming platform optimised for solv-

ing engineering and scientific problems. It is a matrix-based language with a vast library of built-in functions, (MathWorks, 2016). In this thesis, this program was used to analyse processed seismic data. Primarily by finding traveltimes and amplitudes for the refracted events and creating contour plots of these data. The license for MatLab is an academic license intended for use by students at NTNU.

The Petrel E&P Software platform is a complete solution that can be used from exploration to production. It includes workflows for geophysics, geology & modelling, petroleum engineering, drilling and geomechanics (Schlumberger, 2017c). Of these, geophysics was used for interpretation of a horizon and amplitude analysis.

Chapter 4

Available data

The interest in the shallow parts of the subsurface is usually not the reason for acquiring seismic or well data. This is also the case for the seismic data provided for this thesis. Both processed and raw data are used to achieve the results. The 3D seismic data has a low vertical resolution in the shallow parts, due to large minimum offset. The acquisition parameters are not optimised for imaging the shallow subsurface, but the processed 3D cube have recently been processed with the aim to image shallow gas hazards. The LOSEM processing started off as Breistøl (2015) master thesis. Some well logs from neighbouring wells of 2/4-14 are also provided. These logs include gamma-ray readings and velocity measurements.

4.1 3D seismic data, SG9111

The seismic data provided for this thesis are both processed and raw 3D data. Geco-Prakla AS acquired the data for SAGA Petroleum in 1991 with a vessel with dual source and dual streamer. The data acquisition parameters are displayed in table 4.1 and an illustration showing the acquisition configuration is shown in figure 4.1 (LOSEM, 2016).

The seismic data set was acquired with the objective of imaging deep layers and possible hydrocarbon reservoirs at these depths. The minimum offset from acquisition setup is 175 metres, which is too high if the shallow subsurface should be image properly. If the critical angle between the seabed sediments and the water is 50° and the general water depth in the study area is 70 metres, the maximum offset for the primary seabed reflection will then be approximately 167 meters. With the nearest offset, according to acquisition configuration, at

Table 4.1: List of acquisition parameters for the seismic dataset SG9111.

Parameters	
Number of streamers	2
Streamer separation	150 m
Receiver separation	12.5 m
Cable length	3400 m
Nearest offset	175 m
Source interval from flip to flip	50 m
Source separation	75 m
Distance between sail lines	150 m

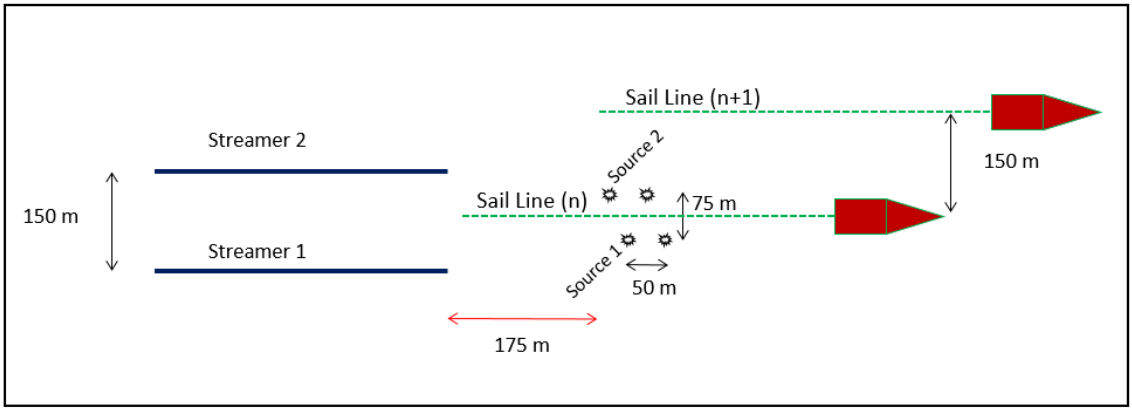

Figure 4.1: Schematic illustration of the acquisition configuration for the 3D seismic data SG9111. The distance between a shot with source 1 (flip) to a shot with source 2 (flop) is 25 m. The green dotted lines indicate different sail lines. Inspired by figure in (LOSEM, 2016)

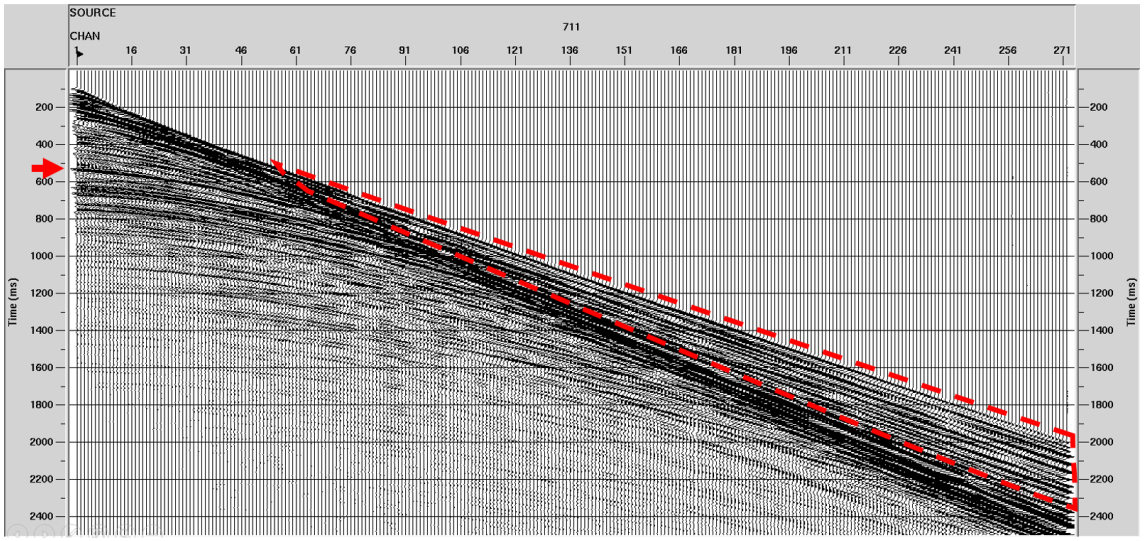

Figure 4.2: Raw shot gather from a location close to the blowout well. Reflection from gas accumulation at 490 m can be seen at 520 ms, marked with red arrow. The strong linear events within the red dashed area at large offsets are interpreted as refracted events.

175 meters the primary seabed principally cannot be recorded by the first receiver. As the depth is 70 metres the seabed multiple arrives approximately 90 ms after the primary.

4.1.1 Raw data

The raw data provided are organised and stored in .SEGY files, one for each sequence going from number 018 to 141. Each of these sequences represents different sail lines. As this is a dual source dual streamer acquisition there are four subsurface lines within each sequence.

Full trace length is 8 seconds which is way higher than the scope of this thesis since the general area of interest is at less than 1 second TWT for the reflections and 2500 ms for the refractions. In this thesis, the focus is on the refracted energy, this is generally the straight high amplitude energy seen at large offsets. To reduce the size of each trace the data is cut at 2500 ms early in the workflow. The refracted energy of interest is then still in the data.

Figure 4.2 show a shot gather at close proximity to well 2/4-14. At this point the traces are already cut at 2500 ms, the gather is high in refracted energy. The linear events within the red dashed area are interpreted as refractions. At 520 ms, marked with red arrow in the figure, one can see a strong reflection, this is the gas accumulation at 490 m. The general quality of the raw seismic data is good.

Figure 4.3 is a brute stack. To create this, simple processing steps are applied prior to

stacking, i.e. top mute, true amplitude recovery, bandpass filter, normal move-out correction and common depth point sorting. The parameters used in these processing steps are based on prior knowledge about the data and area. Well 2/4-14 is located at Common Depth Point (CDP) 2980 and is at the centre of the diffractions with increasing depth, one diffraction is marked with a dashed line in the figure. Diffractions appear as hyperbolic or umbrella shaped events in the seismic section and are caused by the radial scattering of a wave after it meets a discontinuity in the subsurface, in this case, the well (Schlumberger, 2017a). Around the well at 520 ms, the strong reflection caused by the gas is visible, the lateral extent of this anomaly is $\sim$2.4 km. The multiple of this reflection can be seen 90 ms below the primary.

The data was prepared for processing with the geometry setup, 22 sail lines located around the blowout well was further processed. The geometry setup in ProMAX prior to processing was done in collaboration with a fellow student, Elisabeth Grindstad.

4.1.2 Processed data

The LOSEM processing started off as the master thesis of Breistøl (2015) and was processed with the goal of improved imaging of the shallow subsurface, i.e. rock volume down to 1 s two-way traveltime. The processed cube show good multiple attenuation and general good resolution seismic, but at the shallowest parts the resolution is still poor and it is hard to distinguish between reflectors.

In this thesis, the 3D seismic is generally used to interpret a horizon close to the seabed and for a complementary assessment of the results.

4.2 Well data

Available well logs at shallow depths in this area are very limited with gamma-ray readings from various wells and pressure-wave velocity from well 2/4-16. Gamma-ray readings from wells 13 and 16 was shown in figure 2.2 in section 2.3 together with locations on some of the wells. The velocity log is limited at depths from 440 to 1000 metres depth and therefore does not cover all the depths of interest. Knowing the velocities of the formations in the area would be very useful e.g. to estimate depths of refractions/reflections and to make models for seismic modelling.

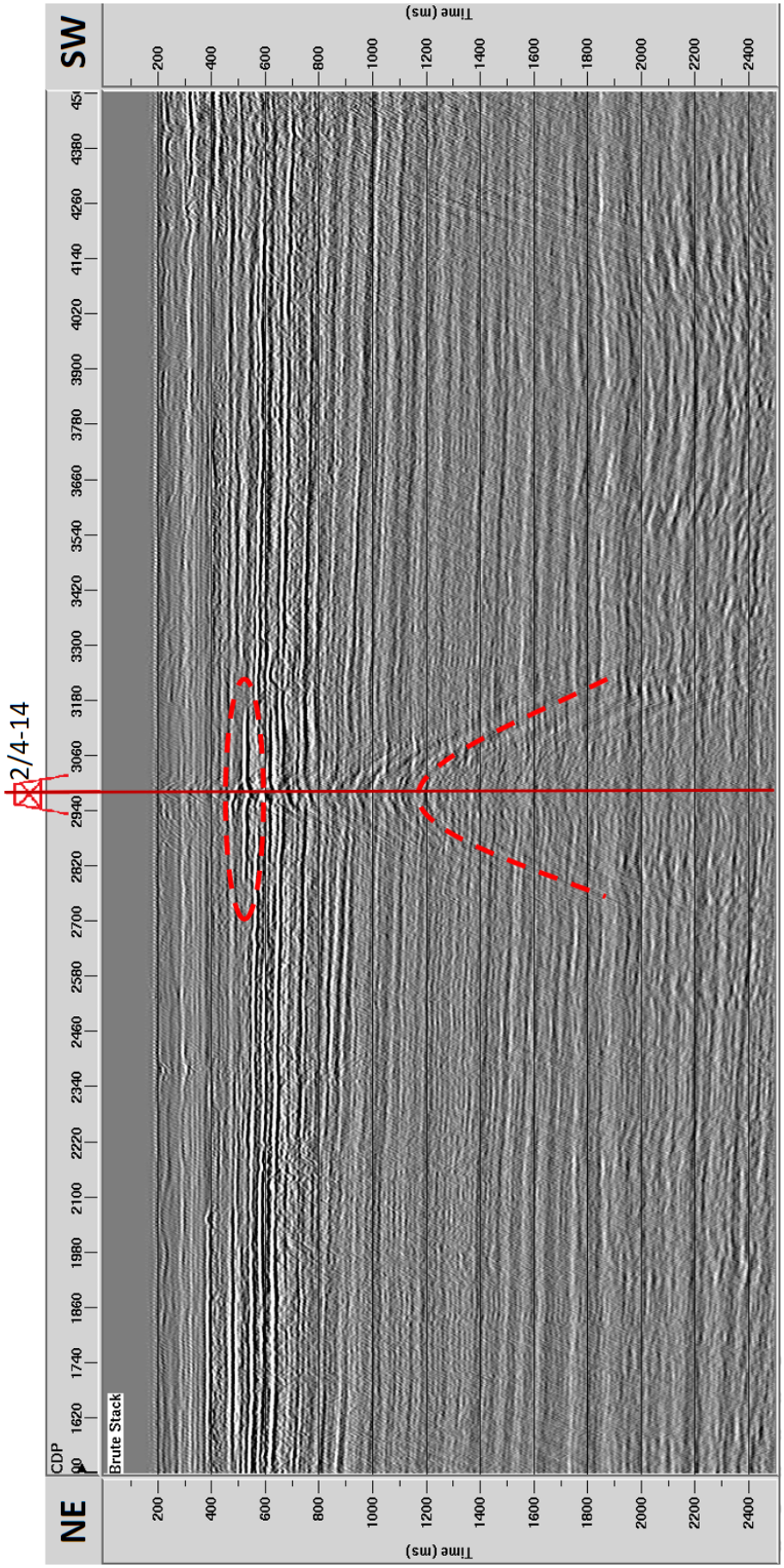

Figure 4.3: Brute stack of SEQ051, CDP range from 1500 to 4500 and correspond to a distance of 18.75 km. The large gas anomaly seen at 520 ms around well 2/4-14 is marked with a dashed ellipse. NE is to the left and SW is to the right.

Chapter 5

Method

In this section, the method used to generate the results are stated. The data was first processed in ProMAX, in two different processing sequences. After the processing in ProMAX, the data was analysed in MatLab.

5.1 Processing ProMAX

The amount of processing done is limited. A very simple processing sequence was set up for this thesis that included top mute, bottom mute, true amplitude recovery and Ormsby bandpass filter. Prior to processing the geometry setup of the raw data was done. Top and bottom mute were applied to mute away possible artefacts in the data. True amplitude recovery was applied with a time power constant of 2. The most important processing step was the Ormsby bandpass filter, different filters were tested and two filters was used further. These were a filter with (2-5-70-80) and (2-5-15-20) Hz limits. The refractions are generally low-frequency waves, hence the low-frequency filters.

The frequency spectra for the raw data is shown in figure 5.1. A small peak of very low frequencies can be seen at approximately 2 Hz, these are usually considered to be because of noise, e.g. swell noise, and should be attenuated during the processing.

The sequences chosen for further processing were chosen based on sail line and distance from the blowout well to get an even distribution of data. Each sequence consists of data from two different sources and two streamers. This corresponds to four subsurface lines. only one of these lines was chosen for each sequence, i.e. source number one and streamer number one.

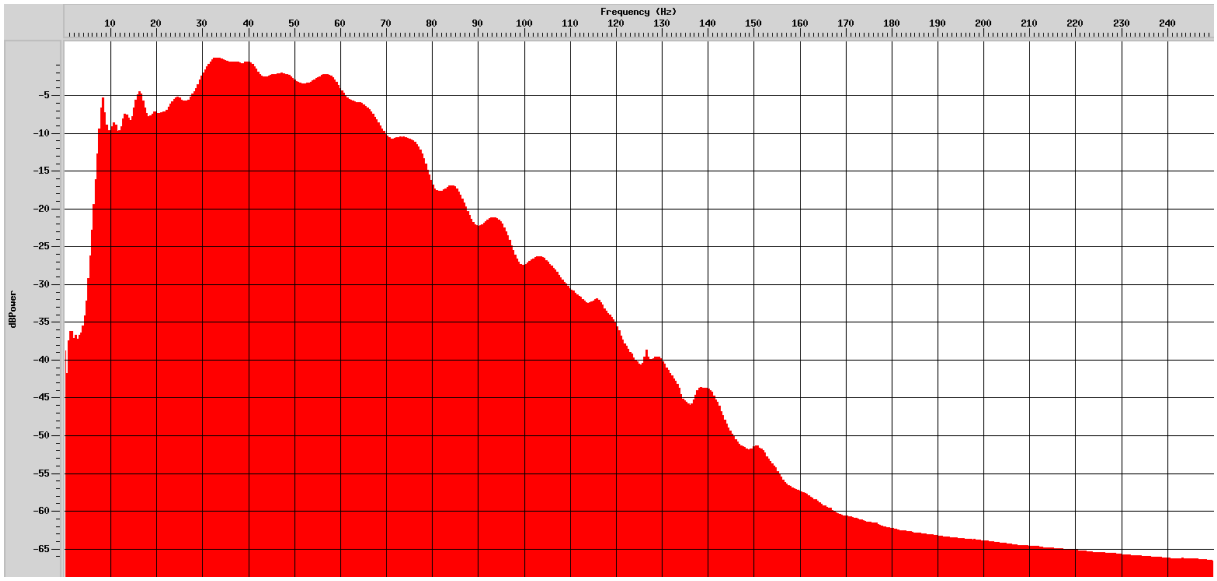

Figure 5.1: Frequency spectrum of the first 2500 ms of the raw data, 20 ensembles are combined for the analysis. The ensembles, i.e. 20 shot gathers, are from a seismic line going through well 2/4-14 (SEQ051).

Table 5.1: List of sequences from the raw data that are processed.

SEQ020	SEQ026	SEQ028	SEQ030	SEQ032	SEQ035
SEQ039	SEQ042	SEQ043	SEQ046	SEQ048	SEQ051
SEQ053	SEQ055	SEQ057	SEQ059	SEQ062	SEQ064
SEQ068	SEQ074	SEQ076	SEQ079		

This reduces the amount of data, but this is still a sufficient amount for this purpose.

The lines processed are listed in table 5.1 and the sail lines are shown in figure 5.2, some of the sequences have been acquired with an opposite sail direction than the rest.

The data was processed twice, each with different bandpass filters. Frequency spectrum after the bandpass filter with limits (2-5-70-80) Hz is shown in figure 5.3. Keeping the same axis limits as the raw spectrum, figure 5.1, the effect of the filter is clear. The little peak at a frequency of approximately 2 is attenuated along with the frequencies above 80 Hz.

Figure 5.4 show a zoomed in section of a shot gather pre- and post-processing. Although the refractions, that are the first linear arrivals at the largest offsets in the gather, seems partially attenuated they are more easily distinguishable from each other. This makes the process of mapping the refractions easier.

The second processing sequence, with the bandpass filter with limits (2-5-15-20) Hz, was also processed without problems. After processing the data from each sequence were stored in .SEGY files for further analysis in MatLab.

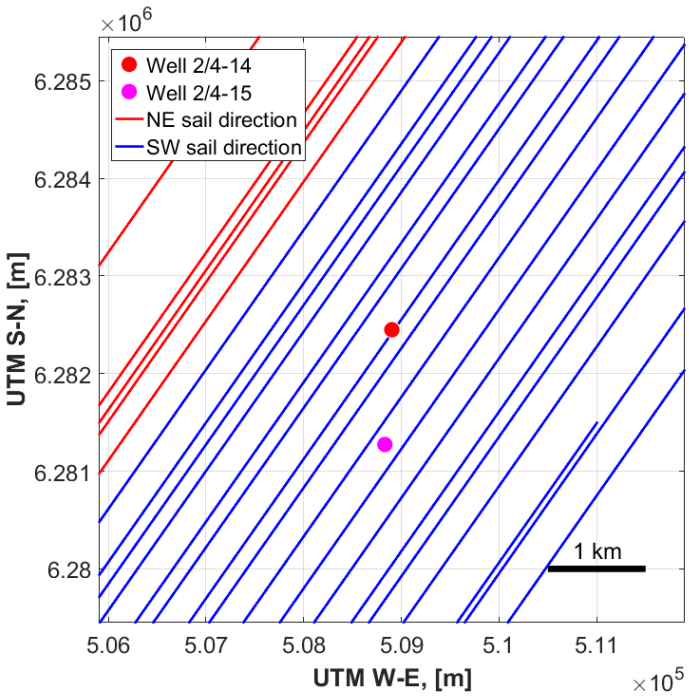

Figure 5.2: The sail lines used for this thesis are shown here as blue and red lines. The red lines have opposite sailing direction than the blue ones. The figure shows a 6 by 6 km^2 grid around the blowout well 2/4-14 with the X and Y-axis in UTM coordinates. UTM W-E increase towards the E and UTM S-N increase towards the north, i.e. north is up, south down, east is right, etc. A one-kilometre scale line can be seen in the bottom right corner.

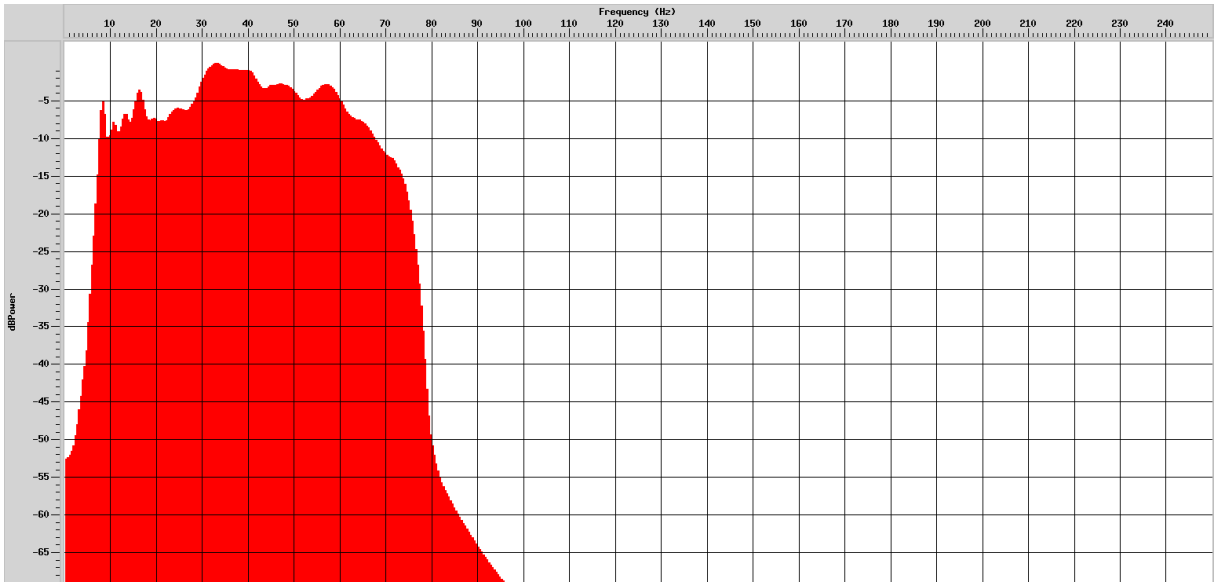

Figure 5.3: Frequency spectrum of the first 2500 ms of the processed data, 20 ensembles are combined for the analysis. The ensembles, i.e. 20 shot gathers, are from a seismic line going through well 2/4-14 (SEQ051).

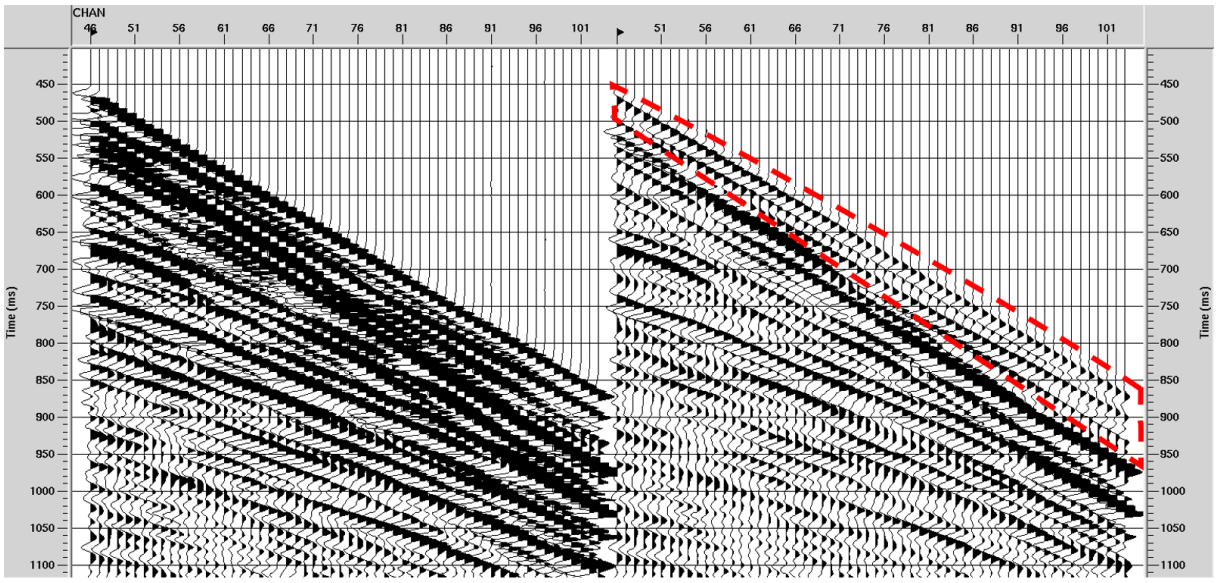

Figure 5.4: To the left a shot gather prior to processing is shown. To the right the same shot gather is shown but after it has been processed. The shot gather originates from SEQ051 close to well 2/4-14. The linear events within the dashed line are interpreted as refractions.

Estimation of intercept traveltimes and velocities above and below a refraction interface is performed in ProMAX. The intercept traveltimes are estimated using the offset, traveltime to refraction and slope of this refraction. These values are put into equation 3.8 and solved for the intercept. To have more robust estimates this process is repeated for several shot-gathers, in this case, ten. located at different areas expected not to be influenced by gas from the blowout. The velocity above the refraction interface can be estimated from the interface reflection traveltime and the velocity below the interface can be estimated by finding the interface head-wave traveltime. For the results in this thesis, these velocities are estimated for ten different shot gathers at different locations believed not to be influenced by gas from the blowout. The velocities are then averaged and rounded to nearest 10 m/s.

5.2 Analysis in MatLab

The .SEGY files containing the data for each sequence were loaded in to MatLab and sorted dependent on which refraction that was to be analysed. For this analysis where the offset is held constant, only one trace from the offset wanted is needed from each gather.

In a 4D case, a cross-correlation technique should be used to find the difference/time-shifts between refractions in base and monitor data. In this thesis, only 3D data is provided and

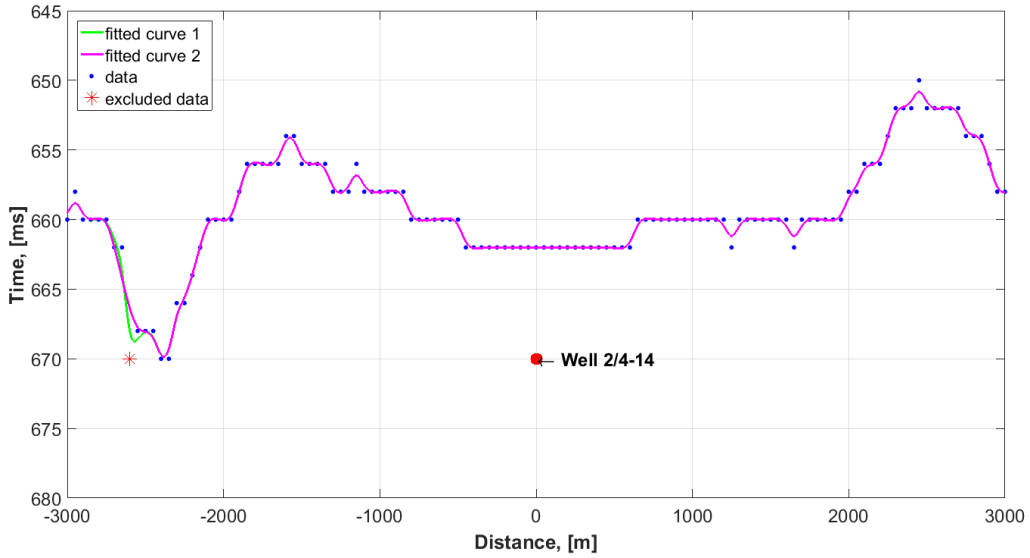

Figure 5.5: Data-points picked by search function along line SEQ051. The initial smoothing spline curve is in green and the second is in magenta. Well 2/4-14 is in the middle at distance 0, increasing distance to the right is in the NE direction and the increasing negative distance to the left is towards SW.

hence a cross-correlation technique would be impossible to apply properly since there is no base survey.

The search function applied here is a straightforward search for the peak of a refraction in a given time-window. As an extra search criteria, a minimum amplitude is set. If the search function finds a peak within the desired search criteria the amplitude and time of this peak is stored, together with the CDP location given in Universal Transverse Mercator (UTM) coordinates.

To ensure that the results are not affected by bad picking by the search function a separate function interpolates the traveltime data for each line and exclude picked data points that do not follow the general trend of the data. Outliers are identified and removed in a two-step process. Initially, data-points that lie at a distance greater than 0.4 standard deviations (std) from a smoothing spline curve through the data are set aside and a new curve is interpolated. The next step was to remove outliers among all the original data-points that lie 1 std from the new interpolated line. Figure 5.5 show the initial smoothing spline curve in green and the second curve in magenta, data-points in blue and outliers removed as red asterisks. It is also possible that the search function fails to find the refraction within the given parameters, then no data is stored for this location. Along the six kilometres shown of line SEQ051 in figure 5.5 data-points for every CDP are found and only one point is excluded here.

Figure 5.6 show the results of the search and outlier detection function. These are the data-

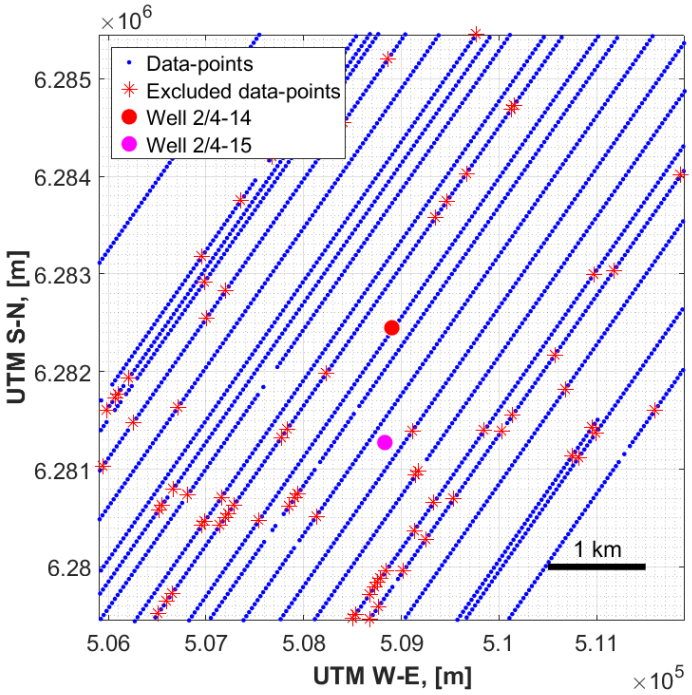

Figure 5.6: Data-points picked by search algorithm are shown here. The picked data-points that are excluded from further analysis are shown as red asterisks. The figure shows a 6 by 6 km^2 grid around the blowout well 2/4-14 with the X and Y-axis in UTM coordinates. North is up, south down, east is right and west is left. An one kilometre scale line can be seen in the bottom right corner.

points for a mapped refraction at 1075 m offset from the first processing sequence.

After the desired data is extracted, it is stored in a suitable manner for surface generation. A 2D grid with coordinates forming a 6 by 6 km^2 area around well 2/4-14 is created and the data is fitted to this grid and linearly interpolated.

From here most of the figures in this thesis are shown in map view with the data in UTM coordinates with well 2/4-14 in the centre and well 2/4-15 approximately 1.2 kilometres south of 2/4-14, like in figure 5.6. The size of the area around the blowout well in the figures is 6 by 6 km^2, UTM S-N increases towards the north and UTM W-E increases towards the east, in other words north is up, south is down, east is right and west is left. A one-kilometre long line is also plotted to easier understand the scale.

Chapter 6

Results

In this section, the main results are shown. Since several figures are relevant for each mapped refraction, to reduce the amount of figures in this chapter many of them are attached in Appendix B. Although most provide good information, the results are explainable with only the figures shown in this chapter. Two different processing sequences with different Ormsby bandpass filters were used, these filters gave different results, with various success. The first processing sequence utilised an Ormsby bandpass filter with limits (2-5-70-80) Hz and the second used (2-5-15-20) Hz. The lowest frequency filter showed the best results with the most pronounced anomalies. A suspected gas anomaly at depth 154-176 metres was successfully mapped. These results were compared with a 4D refraction time-shift analysis done by Zadeh and Landrø (2011) for the same refracted event. Some of the anomalies are possibly associated with the gas at 490 metres, this is discussed in the next chapter. An attempt to locate refractions influenced by the gas accumulation at 840 metres was unsuccessful at this stage, it is still believed that there could be refractions influenced by that gas in the data. A bigger investigation area than the one currently used is needed to visualise this gas accumulation.

6.1 First processing sequence

Figure 6.1 shows a large offset, here 1075 m, comparison for a pair of traces. These are from two different areas, one close to well 2/4-14 and the other approximately 2 kilometres away in the north-east direction. The left comparison show that the difference in traveltime for the different location increase with increasing offset. It is estimated that the apparent average velocity, one

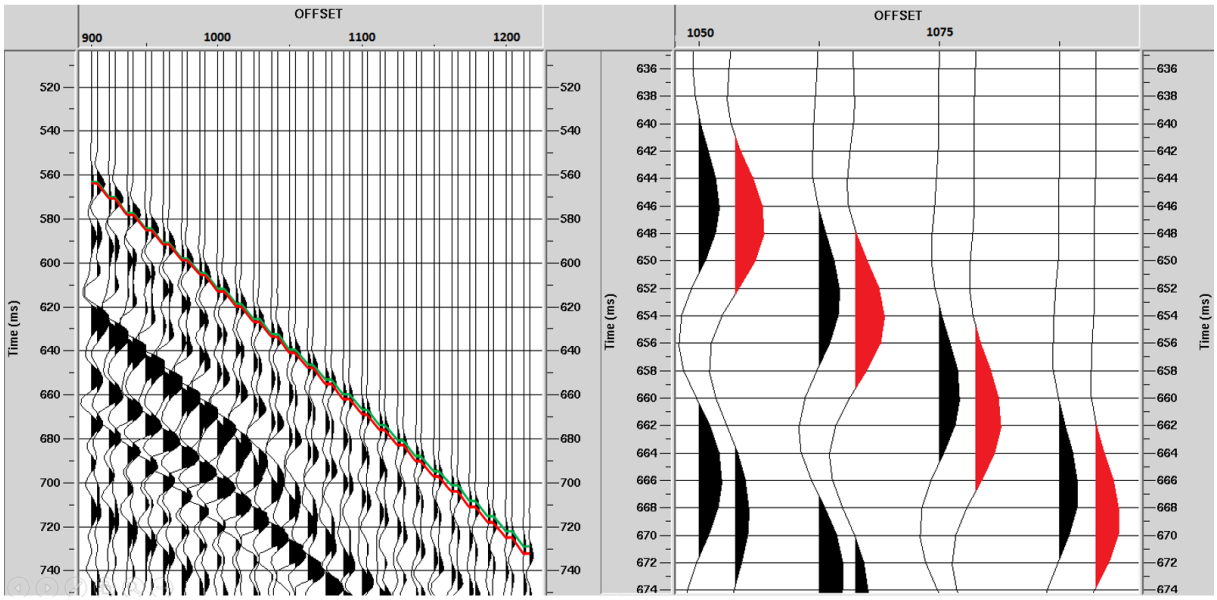

Figure 6.1: Comparison of time to refracted events in the data. Traces from close to and 2 km away from the well are merged and interleaved. The green line between the traces indicate the peak of the refraction for the shot gather far from the well and the red indicates the peak for the gather close/at the well. The figure to the right shows a detailed comparison of the same traces, the refracted event close to the well is shown in red. A time difference of approximately 2 ms can be observed.

over the slope of the refraction, is 1780 m/s for this event. It can also be seen that the strong events that start at 625 and 650 ms in the first trace show no traveltime difference.

Important to note that this is not timelapse data, the traveltime difference observed is merely the difference between two different locations, so the cause for the difference can be many things. When it is assumed that the layers are horizontal, the lithology constant and the pressure regime is constant it can be said that the traveltime difference observed is caused by fluid differences.

In figure 6.1 the first trace in each trace pair is from a shot gather approximately 2 kilometres from the well and the second is from a shot gather close to the well. Note, the shots are actually far from the well, but the common depth-point for 1000 m offset are close to, and 2 km away from the well. The close comparison between the traces to the right in figure 6.1 show that for offset 1075 m the traveltime difference is 2 milliseconds.

The first arrival at 1075 m offset is interpreted as a refraction and the traveltime to this refraction is mapped and the results are shown in figure 6.2, data-points used for the surface interpolation was previously shown in figure 5.6 in section 5.2. Close to 2/4-14 there is a slight increase in traveltime compared to the general traveltime in the plot. The highest traveltimes are located as a large anomaly south-east and two smaller ones west of the wells.

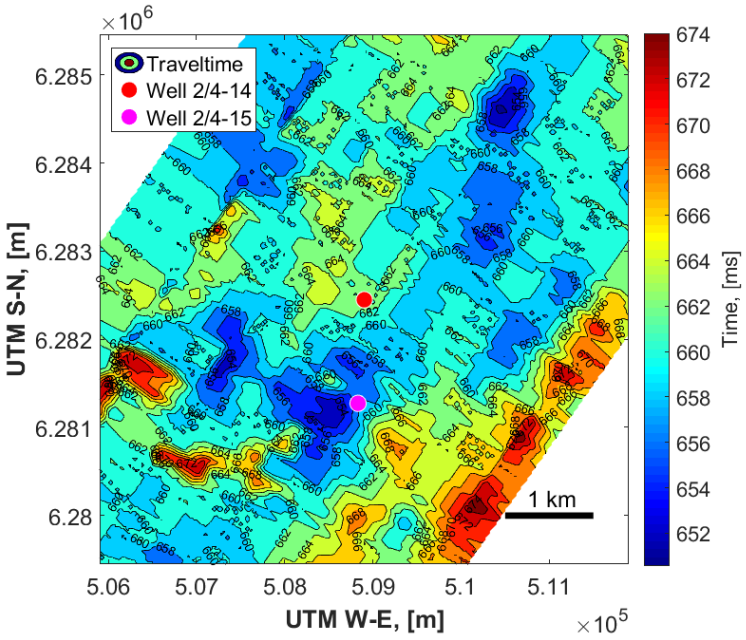

Figure 6.2: Contour plot of traveltime to the first arriving refracted event at 1075 m offset. The Ormsby bandpass filter used during processing is (2-5-70-80) Hz.

Figure 6.3 show the corresponding amplitude data of the mapped refraction. The largest amplitudes seem to correspond well to the largest traveltime anomalies. On closer inspection of CDP gathers it is determined that on the locations of these strong anomalies the 1780 m/s refraction is caught up and overlaps with another refraction with an apparent average velocity of 1850 m/s and stronger amplitudes. This means that when the traveltime difference is too large another refraction is mapped, but the traveltime should still be the same or higher.

It is expected that this refraction corresponds to a shallow interface, possibly a sand layer. The seismic section in figure 6.4 show stronger amplitudes close to well 2/4-14 at 220 milliseconds that might be of interest.

The intercept traveltime of the refraction is estimated to be approximately 70 to 80 milliseconds. Given that we can estimate the velocity above and below the interface, the depth of the refraction interface can be estimated with the refraction intercept time.

From the interface reflection traveltime, the velocity above the interface can be estimated and the velocity below the interface can be estimated from the interface head wave traveltime i.e. slope of the refraction. It is estimated that the average velocities above and below the interface are 1650 and 1780 m/s respectively. Using the velocities above, the estimated intercept

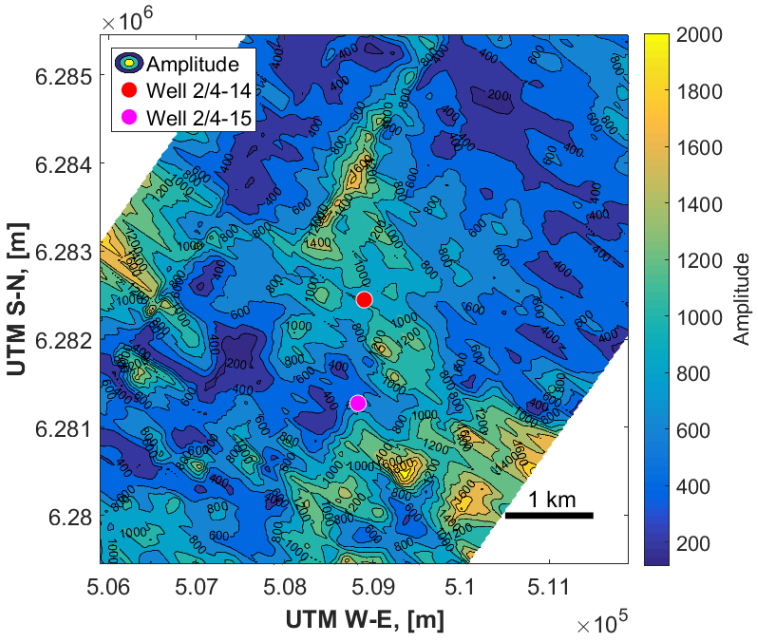

Figure 6.3: Amplitude contour plot of the first arriving refracted event at 1075 m offset. The Ormsby bandpass filter used during processing is (2-5-70-80) Hz. Amplitudes here correspond to the traveltime contour plot shown in figure 6.2.

traveltimes and the intercept in equation 3.8 possible depths of the anomaly are estimated to be between 154 to 176 metres.

Using the estimated velocities and depths above, the offset and equation 3.9 the time-shift, or in this case, traveltime difference can be estimated. Assuming a velocity change of -50 m/s, i.e. around -3%, for an anomaly the traveltime difference is estimated as 5 ms for H=154 m and 3.2 ms for H=176 m. The shallower the refraction layer is, the more sensitive it is to velocity changes. In this area, there are no velocity well logs this shallow that can confirm the depth and velocity of the potential sand layer.

The processing sequence utilised for the results in this section conserves relatively high frequencies. This high-frequency data is more influenced by depth differences and irregularities in the subsurface, i.e. the surface causing the refraction is not horizontal. To take this into account a reflector in the 3D seismic cube is interpreted and used to create a base for the refraction data. Because of high minimum offset during acquisition, the shallow resolution is poor and the first reflector that is interpretable is located at around 350 milliseconds, the interpreted horizon can be seen as the pink line in figure 6.4. An isochrone map of the interpreted horizon can be seen

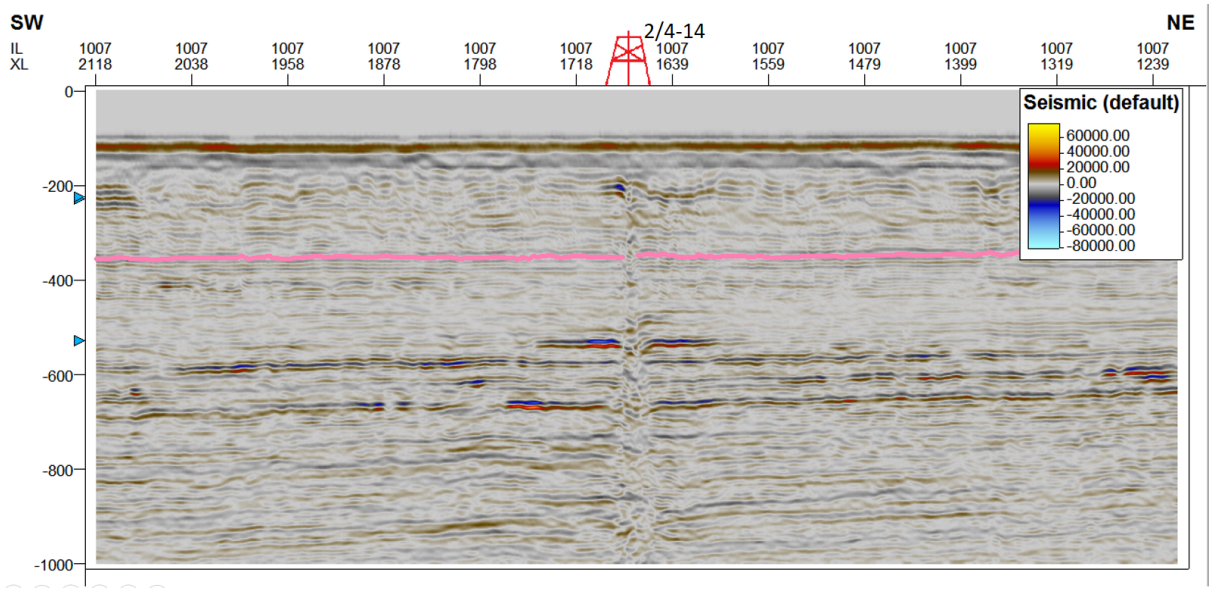

Figure 6.4: Seismic section that stretches 11 kilometres from left to right, well 2/4-14 is located in the middle. At 220 ms there are some stronger amplitudes close to the well. Gas anomaly at 520 milliseconds is easily seen in the middle of the figure. The pink horizon at 350 ms is interpreted throughout the cube.

in figure 6.5. Notice the area in the SE, here there is a large area with increased TWT.

To use this surface as a base for the refraction data it needs to be converted to refraction traveltime. The traveltime of an refracted event is given in equation 3.8, substituting in $T_0 = \frac{2H}{V_1}$ we get

$$t = \frac{X}{V_2} + T_0\sqrt{1 - \left(\frac{V_1}{V_2}\right)^2}, \qquad X \geq X_c, \tag{6.1}$$

Where T_0 is the two way traveltime (TWT) of the corresponding reflected surface.

To be able to apply this equation, the interpreted horizon is moved up to match the estimated TWT of the refraction approximately 500 metres south-west of well 2/4-15, where zero time-shifts are expected. Using the interpreted horizon as T_0, $V_1 = 1650$ m/s, $V_2 = 1780$ m/s and offset $X = 1075$ metre in equation 6.1 we get the surface shown in figure 6.6. The two-way traveltime for the reflection is not influenced by the velocity below the interface, the amplitude of reflection is. The estimated traveltime for the refraction based on this reflection surface is calculated based on a constant estimated velocity. Because of this, we get an estimation of the refracted traveltime unaffected by velocity differences in the subsurface. Velocity differences can be caused by e.g. different lithologies, different pressure regimes and different fluids.

In figure 6.6 it can be seen that the traveltime differences are relatively small with one large exception to the SE, in this area the estimated traveltime is around 662 ms.

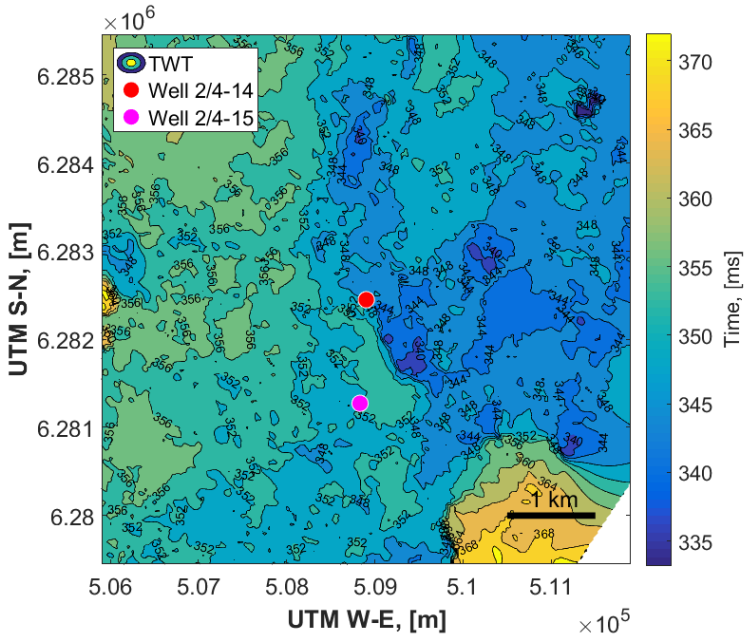

Figure 6.5: TWT of an interpreted surface in petrel, this is the first reflector in the 3D seismic cube that is possible to interpret throughout the cube. This is also the pink horizon marked in figure 6.4.

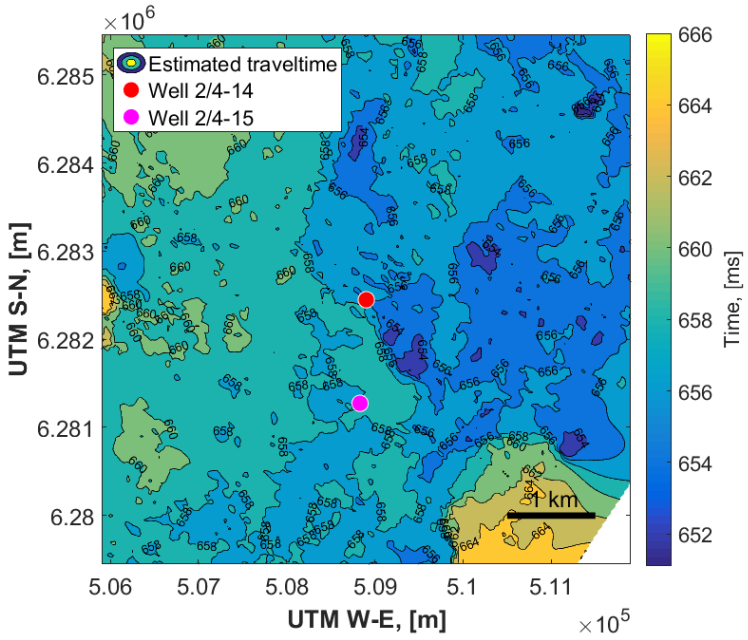

Figure 6.6: Estimated refracted traveltime for the interpreted horizon seen in figure 6.5.

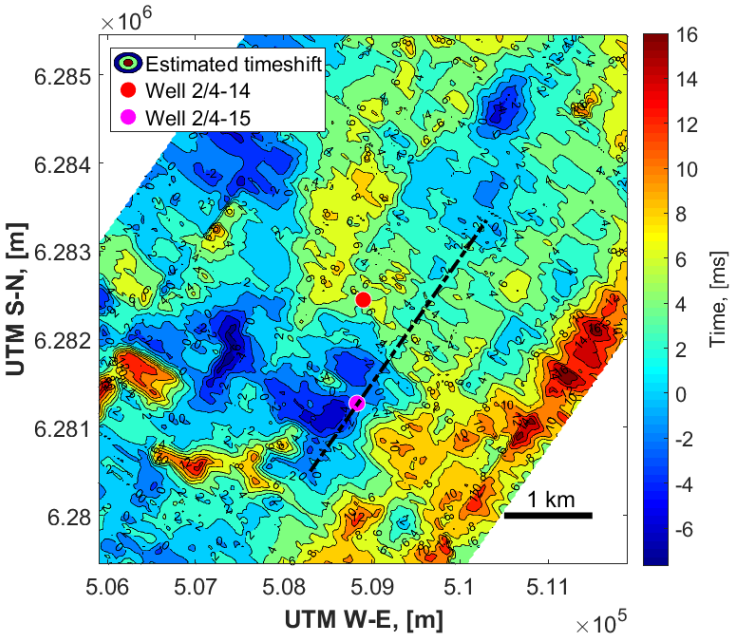

Figure 6.7: Estimated time-shift for the refraction at 1075 m offset based on an estimated base survey and the refraction traveltime as monitor (base: figure 6.6 and monitor: figure 6.2). The black dotted line going through well 2/4-15 indicate the section in which Zadeh and Landrø (2011) did a 4D refraction time-shift analysis.

Using the estimated traveltime for the refraction in figure 6.6 as a baseline and the original results in figure 6.2 as monitor, an estimation of time-shifts for the refraction can be calculated. Figure 6.7 show the estimated refraction traveltime time-shift for the first arriving refraction at 1075 m offset. The time-shifts observed here is assumed to be caused by lithology and fluid differences in the subsurface. The large anomalies identified earlier in figure 6.2 are still present, but less pronounced here. The large area in the SE with the highest traveltimes in the monitor shows the biggest differences, here most of the high traveltimes have been lowered. This is not the case for the estimated time-shift to the east where it has become more definite. Around well 2/4-14 time-shifts of approximately 4-6 milliseconds can be observed, but these time-shifts are also seen many places throughout the figure.

Zadeh and Landrø (2011) found refraction time-shifts for offsets ranging between 1000 and 1150 metres along a 2D seismic line, this line is marked as the dotted line in figure 6.7. The base survey was acquired in 1988 before the drilling of 2/4-14 and the monitor in 1990 after the blowout. They find consistent time-shifts of up to 4 milliseconds, with the maximum close to the projection of the blowing well. To compare their results with the results found here a curve

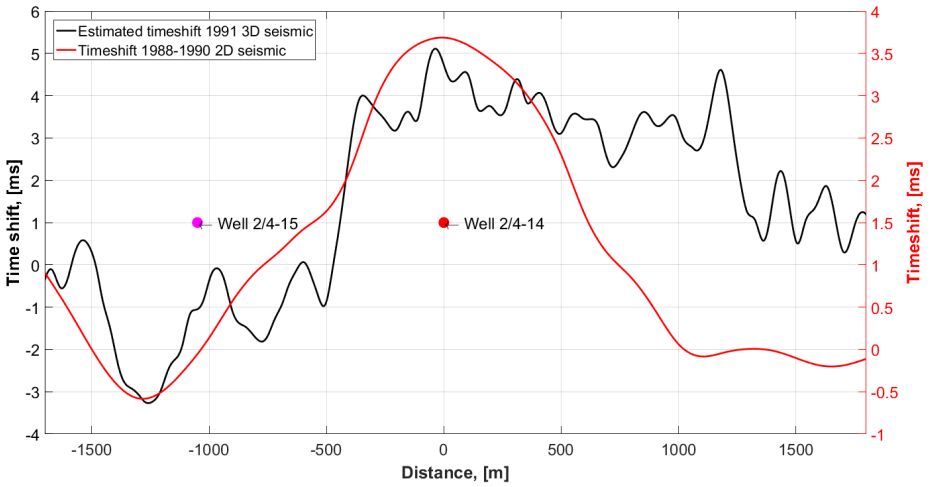

Figure 6.8: Estimated refraction time-shift from 1991 3D seismic data after processing with (2-5-70-80)Hz bandpass filter, compared with 4D refraction time-shift analysis by Zadeh and Landrø (2011). The data are compared along the same 2D line which can be seen in figure 6.7, the points along this dotted line that are closest to the wells 2/4-14 and 2/4-15 are marked. The different colored Y-axis correspond to their similar colored graph.

across their scattered data-points is manually interpolated visually. A copy of their figure and the interpolated curve can be seen in appendix C.

The estimated refraction time-shift along the dotted line in figure 6.7 can be seen in figure 6.8. On a separate Y-axis the interpolated curve from Zadeh and Landrø (2011) is plotted for comparison. Southwest of 2/4-14, towards 2/4-15, the two results show very similar trends, but north-east they differ from each other. Extending the line from the estimated time-shift data in the NE direction it eventually reaches around zero, but around 600 metres further from the well than the actual time-shift data. Interesting to see is the negative time-shift observed close to 2/4-15 for both results, they also both have their maximum time-shift close to the projection of the blowout well. Also, note that the y-axis on each of the two different data is very similar.

An attempt to map more refractions for this processing sequence was unsuccessful, either the refraction was difficult next to impossible to map or the results were inconclusive with no clear anomalies.

6.2 Second processing sequence

The second processing sequence used an Ormsby bandpass filter with limits (2-5-15-20) Hz. The idea is that the subsurface interfaces appear flatter/more horizontal with the low frequency

data. In addition, the refractions generally have a lower frequency content than the reflected waves.

There is a known gas anomaly at 490 metres depth, seen as the strong reflection at 520 ms close to the blowout well in figure 6.4. It can also be seen in the figure that the gas accumulation yields a negative reflection. A negative reflection coefficient is caused by a decrease in impedance from above to below an interface. If this decrease is caused by velocity decrease no head-wave is generated at this interface.

Hansteen et al. (2010) measure the time-shift of first arrival head-waves from a refraction layer below a reservoir. Their time-lapse study is successful and gives good hopes for finding the 490-metre gas anomaly with this method. It is expected that tuning also increase the amplitude of the refraction, making it appear stronger in the shot gather. From the gamma-ray log in figure 2.2 it can be seen that the layer at 490 meters is approximately 10 metres thick.

Simple calculations with a two-layered model indicate that a refraction from a depth of 500 metres will appear on the gather at offset over 2700 metres, the critical offset, with $\theta_{crit} = 70°$. In other words, refractions from depths of 500 metres might be visible from around channel 200 and up in the shot gathers in the seismic data.

Figure 6.9 show a shot gather from a location close to well 2/4-14 with the largest offsets available. Five easily seen refractions arrive at channel 272 at traveltimes 2010, 2140, 2240, 2350 and 2450 ms. A sixth refraction that arrives before these five is barely visible at 1950 ms.

To check for possible traveltime differences of refractions at difference offsets, a simple method of plotting a single trace at a certain offset for every CDP gather in one sequence can be used. Since the goal is to potentially map a refracted event influenced by the gas at 490 metres a very large offset should be picked. As shown in section 6.1 figure 6.1 the traveltime difference increase with increasing offset, thereby the largest offset available, i.e. 3563 metre, is picked for further analysis.

Figure 6.10 show every trace at 3563 metre offset for each CDP gather. The seismic data here is from SEQ051 that have a sail line that crosses over well 2/4-14. The wiggle traces have been gained up significantly to make the refraction at 1950 ms visible. A variable density plot of the same traces is shown in figure A.1 in Appendix A, traveltime differences are also evident here. Further on from here the refractions from first to the last arrival are numbered from 1 to 6, respectively.

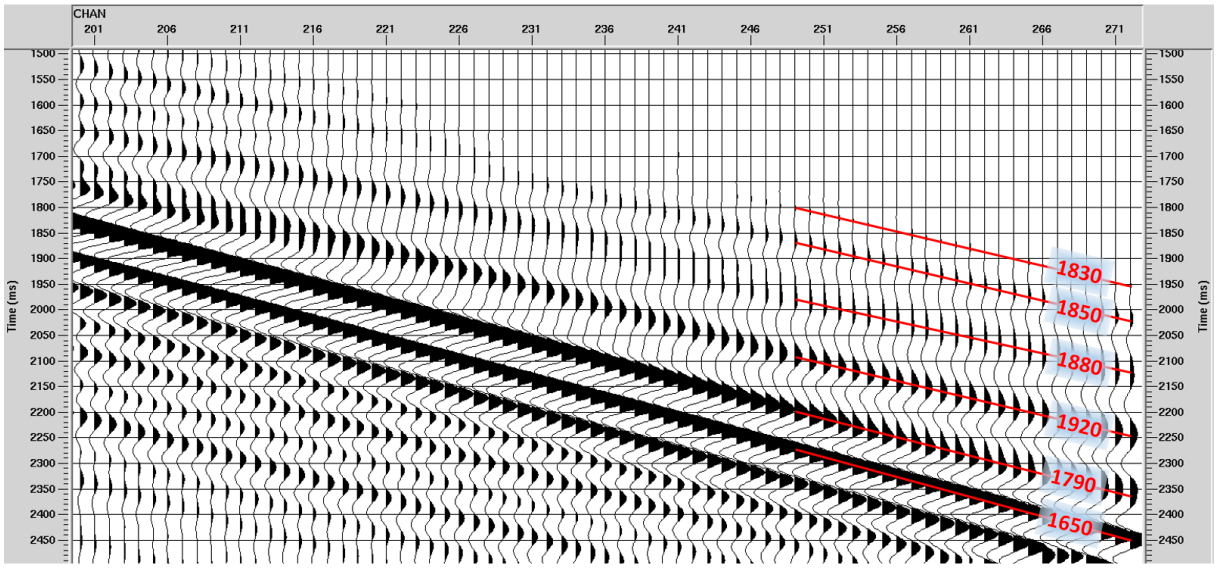

Figure 6.9: Shot gather from a location close to well 2/4-14 along SEQ051. The offset ranges from 2675 to 3563 metres. High amplitude linear events seen here are interpreted as refractions. The apparent average velocities marked for the six first arriving refractions are given in m/s.

Table 6.1: Average apparent velocities of the six first refractions arriving at 3563 m offset, seen in figure 6.10.

Refraction number	Approximate arrival time [ms]	Velocity [m/s]
1	1950	1830
2	2010	1850
3	2120	1880
4	2240	1920
5	2350	1790
6	2450	1650

The average apparent velocity of the six refractions is shown in table 6.1. Notice that the two latest arriving refractions show the lowest velocities. Normally in reflection seismic, the first arrivals have the lowest velocities and the first reflection always corresponds to the shallowest layer. For the arriving refractions, the first arriving one does not necessarily correspond to the shallowest layer.

The first refraction has a very low amplitude and from figure 6.10 it can be seen that close to the well it becomes very irregular or vanishes. The same refraction close to the well might be the stronger arrival at around 2000 ms, which would imply a traveltime difference of approximately 50 ms. This was not considered and the search function failed to find the refraction close to the well. Figure 6.11 show the picked data points and in an approximately 1.2-kilometre radius around well 2/4-14 no refraction was found.

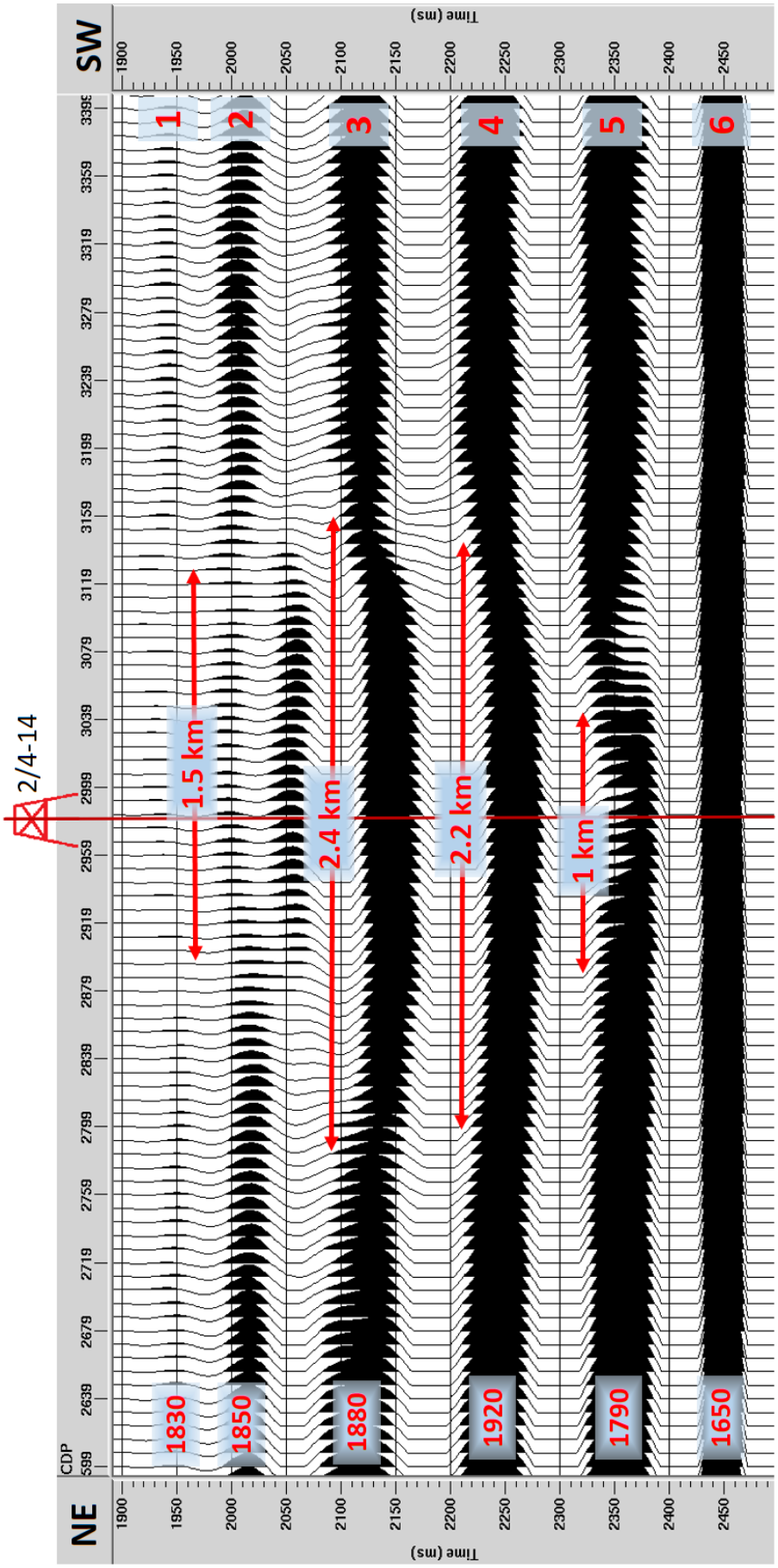

Figure 6.10: Trace at offset 3563 m for each CDP gather along line SEQ051, this line pass over well 2/4-14. The well is situated at approximately CDP 2980 in the middle of the figure, the distance from left to right is 5 kilometres. The traces are gained up significantly to be able to see the first refraction at 1950 milliseconds. Refractions are numbered from 1 to 6 to the right and their apparent average velocity is to the left in m/s. The sail direction is SW, hence SW is to the right and NE is to the left.

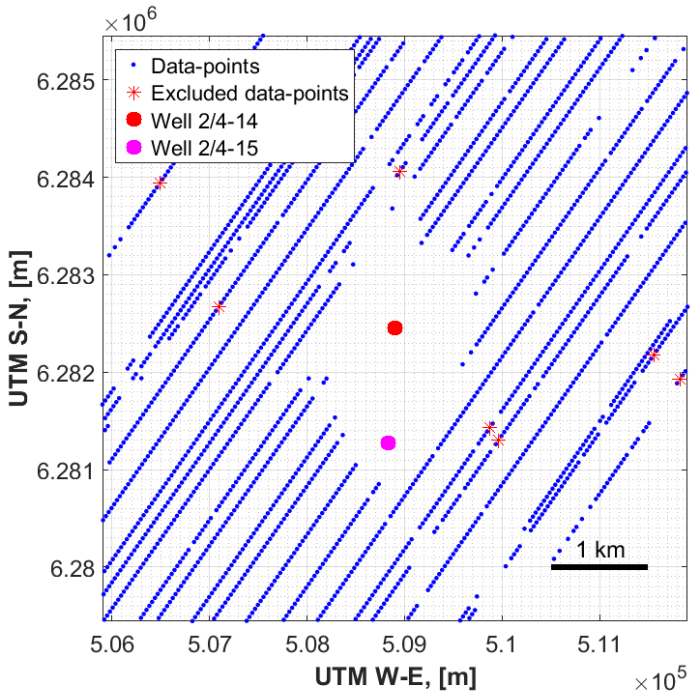

Figure 6.11: Data-points found by the search function for the first arriving refracted event at 3563 m offset. Notice that no data-points are picked around well 2/4-14. The picked data-points that are excluded from further analysis are shown as red asterisks.

The second refraction generally arrives at 2000 ms, but close to well 2/4-14 at that time a much lower amplitude refraction is seen. It is determined that the refraction corresponding to the 2000 ms refraction around the well is the one that arrives at approximately 2050 ms. At the transition between the general traveltime and the 50 ms slower arrival, the traces are inconsistent and the search function is unable to choose peak. As a result, seen in figure B.3 in Appendix B, data points are picked close to the well and generally everywhere except for an area approximately 600 metres in radial distance from the well.

A clear anomaly around well 2/4-14 can be seen in figure 6.12. The traveltime of the second refraction around the well here is approximately 50 ms higher. In the amplitude contour map in figure B.4 the area around the wells shows the lowest amplitudes. The lack of data in the transition zone creates some uncertainties about the size of the anomaly, but it appears to be approximately 1 km^2.

The third refraction show high amplitude and clear and smooth trend between the different CDP's, see figure 6.10. In figure B.5 data-points are consistently picked along this line (line SEQ051), the dotted line that crosses over well 2/4-14.

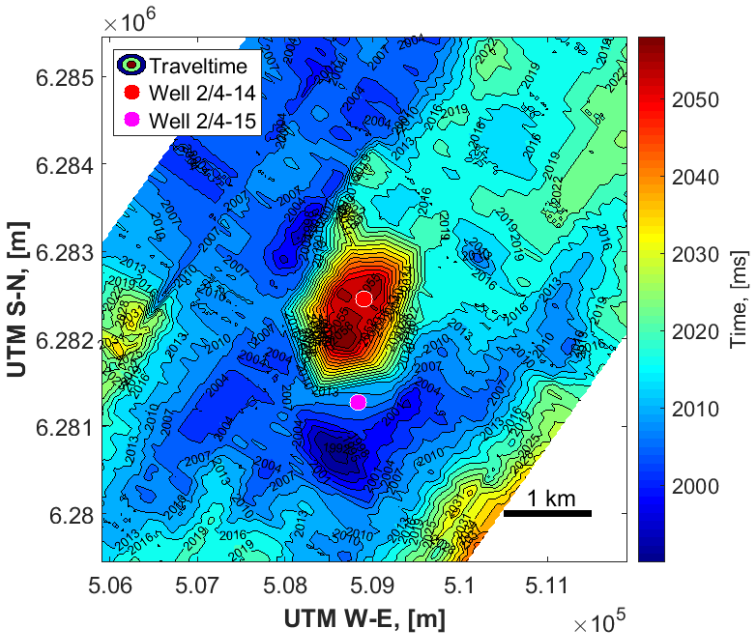

Figure 6.12: Traveltime to the second arriving refracted event at 3563 m offset. The bandpass filter used during the processing is (2-5-15-20) Hz.

Traveltime contour map for the third event is shown in figure 6.13. A large anomaly is visible around the well, the elliptical anomaly is approximately 2.4 km in the NE-SW direction and 1.6 km in the NW-SE direction. The anomaly show traveltimes approximately 25 ms slower than the general traveltime. Comparing the traveltime with the amplitude contour plot in figure B.6 in Appendix B the general trend is that the stronger amplitudes corresponds to the highest traveltimes and vice versa.

The fourth refraction seen in figure 6.10 show a similar trend as the third, but appear less pronounced and smaller in extent. Because of the smooth transitions between CDP's and similar looking waves this refraction is picked with confidence throughout the data. Figure B.7 show how nearly all the lines are complete with data points.

The anomaly seen around well 2/4-14 in figure 6.14 is noticeable smaller than the anomaly of the third event in figure 6.13. This elliptical anomaly is approximately 2.2 km in the NE-SW direction and 1.2 km in the NW-SE direction. The anomaly show traveltimes approximately 20 ms slower than the general traveltime. A similar relation between amplitude, figure B.8, and the traveltime can be seen here as well, but not around 2/4-14.

The fifth refraction seen in figure 6.10 shows a general strong amplitude and an increased

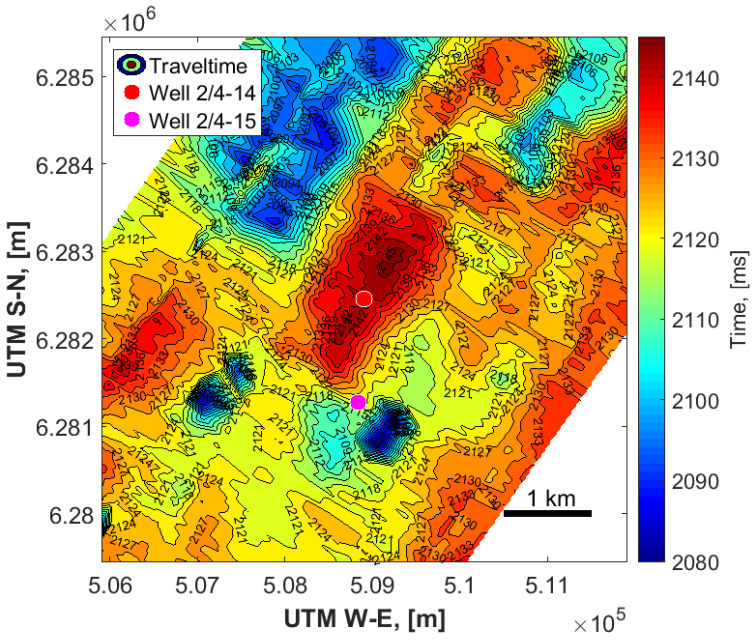

Figure 6.13: Traveltime to the third arriving refracted event at 3563 m offset. The bandpass filter used during the processing is (2-5-15-20) Hz.

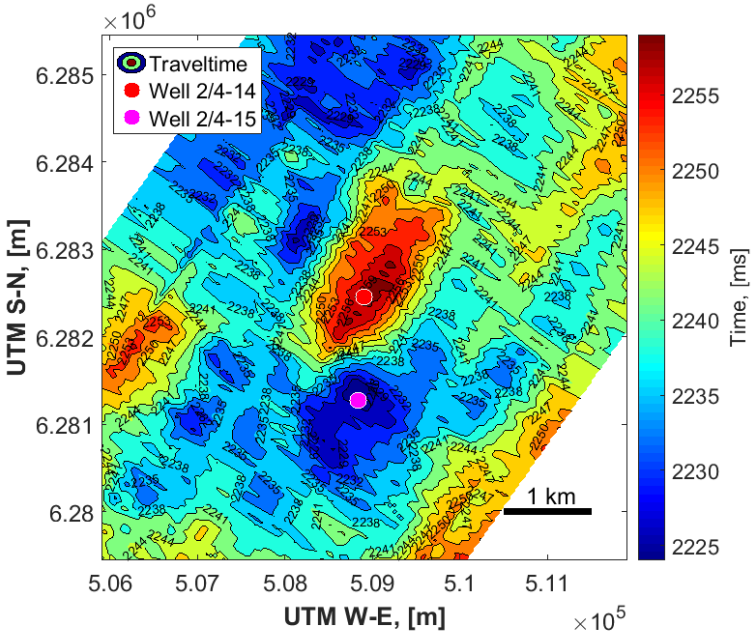

Figure 6.14: Traveltime to the fourth arriving refracted event at 3563 m offset. The bandpass filter used during the processing is (2-5-15-20) Hz.

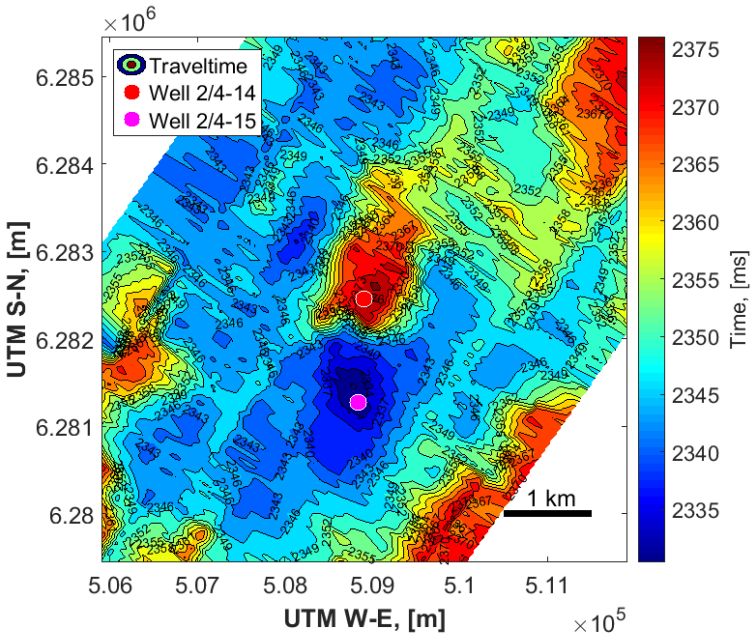

Figure 6.15: Traveltime to the fifth arriving refracted event at 3563 m offset. The bandpass filter used during the processing is (2-5-15-20) Hz.

traveltime to the peak of wavelet near the blowout well.

The resulting traveltime contour plot is seen in figure 6.15 show a much smaller anomaly around the well than the other refractions mapped. This anomaly appears almost circular in shape with a diameter of approximately 1 km, and area of 0.8 km^2. The general traveltime difference between the anomaly and the rest is about 30 ms. In this case, the higher amplitudes, see figure B.10, correspond to the lowest traveltimes and around 2/4-14 we see the lowest amplitudes.

The sixth refraction seen in figure 6.10, at 2400 milliseconds, show no indication of a difference in traveltime across the section, this event is therefore not analysed further.

The method used for the refractions above clearly works as large anomalies are found around the blowout well. Following this, multiple refractions at different offsets have been mapped. The results of most of these refractions are inconclusive. Although the refractions are mapped properly no clear significant anomaly around the blowout well, like the ones already shown, are found and therefore they are not shown here.

The refracted event at 1075 m offset mapped for the first processing sequence is also mapped here. The data-points found and excluded by the search algorithm is shown in figure B.11 and

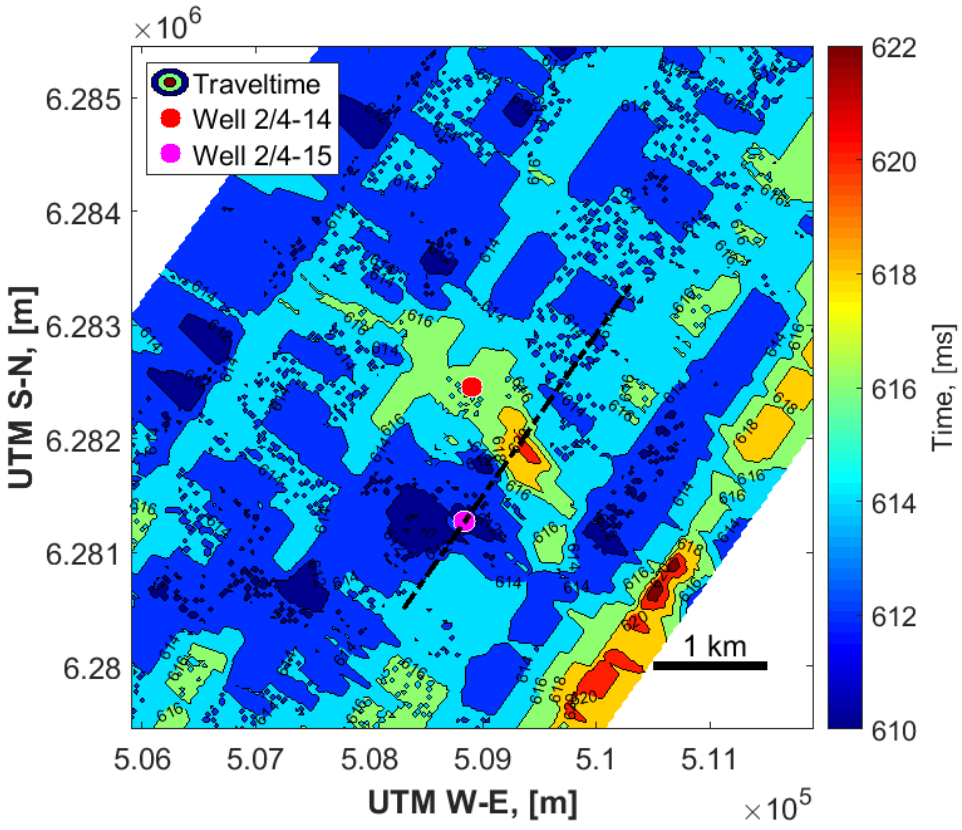

Figure 6.16: Traveltime to the first arriving refracted event at 1075 m offset. The bandpass filter used during the processing is (2-5-15-20) Hz.

the amplitude contour map in figure B.12. In figure 6.16 an anomaly around 2/4-14 is evident, with the maximum time-anomaly south-east of the blowout well. The general traveltime difference between the anomaly and the rest is about 6 ms.

The traveltime of the refraction along the dotted line shown in figure 6.16 can be seen in figure 6.17. As earlier the results from the refraction traveltime are plotted as the black line with the corresponding black Y-axis and the results from Zadeh and Landrø (2011) with the red colour. Both results show the same trends with lowest traveltimes and time-shifts close to 2/4-15 and the maximum close to the projection of well 2/4-14.

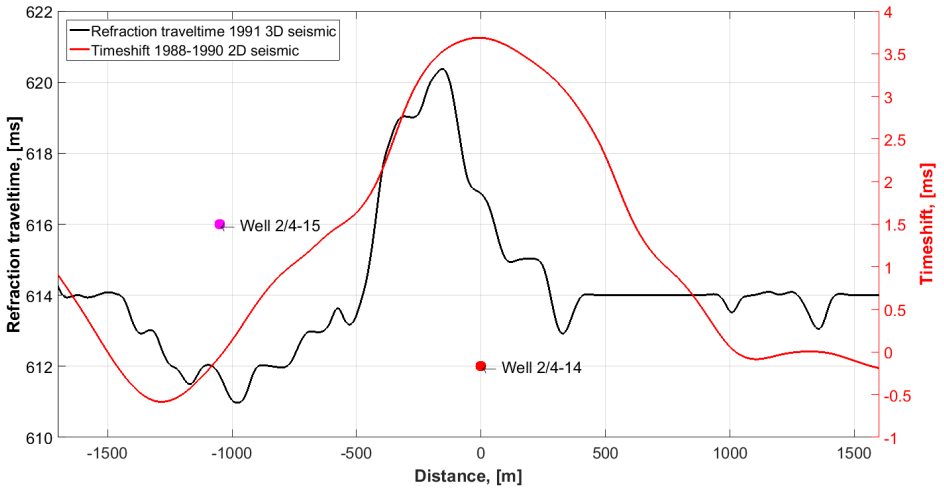

Figure 6.17: Refraction traveltime from 1991 3D seismic data after (2-5-15-20)Hz bandpass filter compared with 4D refraction time-shift analysis by Zadeh and Landrø (2011). The data are compared along the same 2D line that can be seen in figure 6.16, the points along this dotted line that are closest to the wells 2/4-14 and 2/4-15 are marked. The different coloured Y-axis correspond to their similar coloured graph.

6.3 Migration paths

It is believed that tunnel valleys in this area might act as migration paths for gas from the blowout. Halvorsen (2012) map shallow buried tunnel valleys in the central North Sea, that includes the area around the blowout. Mapped tunnel valleys at the depth of interest in this thesis are shown in figure D, of all these tunnel valleys number V13, V16, V17 and V18 are used further for comparison. These are mapped between 180 and 400 ms TWT, but more exactly at which TWT each individual tunnel valley is mapped is unclear.

Tunnel valleys have a different infill than the surrounding lithology and hence also normally a different velocity. Halvorsen (2012) determines that the infill in these tunnel valleys show very small velocity contrast with the surrounding layers. These small differences might be observable with the refraction traveltimes found for the refraction at 1075 m offset.

Figure 6.18 show the estimated refraction time-shift for the first processing sequence, with (2-5-70-80) Hz filter, and the four of the tunnel valleys mapped in Halvorsen (2012). There is some overlap between some of the valleys, especially between V13 and V17. It does not appear that V16 and V18 have any effect on the estimated refraction time-shift, but there appears to be a slight correlation with V13 and quite a clear correlation with V17. East in the figure V17 follows the high time-shifts observed in that area.

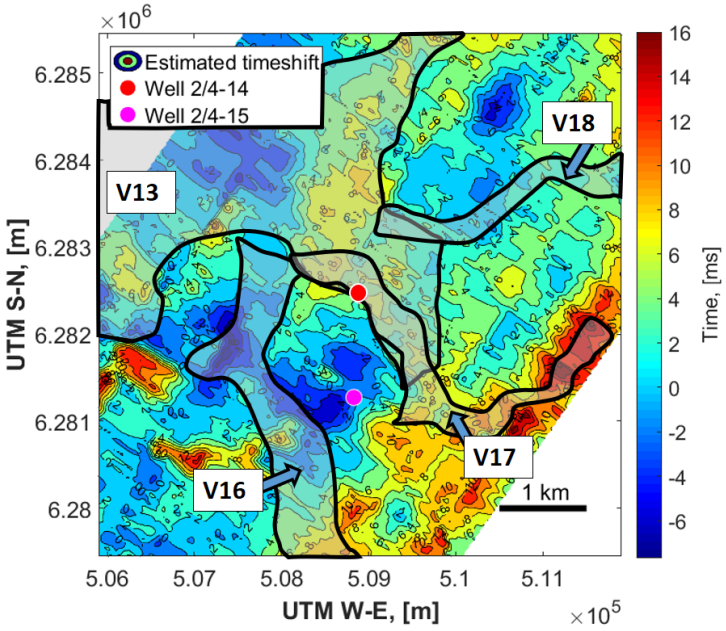

Figure 6.18: Estimated refraction time-shift to the first arriving refracted event at 1075 m offset. The bandpass filter used during the processing is (2-5-70-80) Hz. Tunnel valleys from Halvorsen (2012) are superimposed on top of the estimated refraction time-shift contour plot.

Figure 6.19 show the refraction traveltime compared with the tunnel valleys. Same as for the estimated time-shift V16 and V18 does not appear to have any effect on the traveltime. Both V13 and V17 covers the gas anomaly, but V17 appears to follow and overlap with more of the higher traveltimes to the east.

The Tunnel valleys in Halvorsen (2012) was mapped interpreting horizontal time-slices through a 3D cube. A similar process is used here, with RMS amplitude with a 10 ms time-window, to see if amplitude differences match the gas anomaly seen in figure 6.16. Figure 6.20 show RMS amplitude at 224 ms TWT together with an interpretation of the outline of the gas anomaly. The anomaly is interpreted approximately along the 616 ms contour line. The higher RMS amplitudes in the proximity of the blowout well corresponds nicely to the red circuit line.

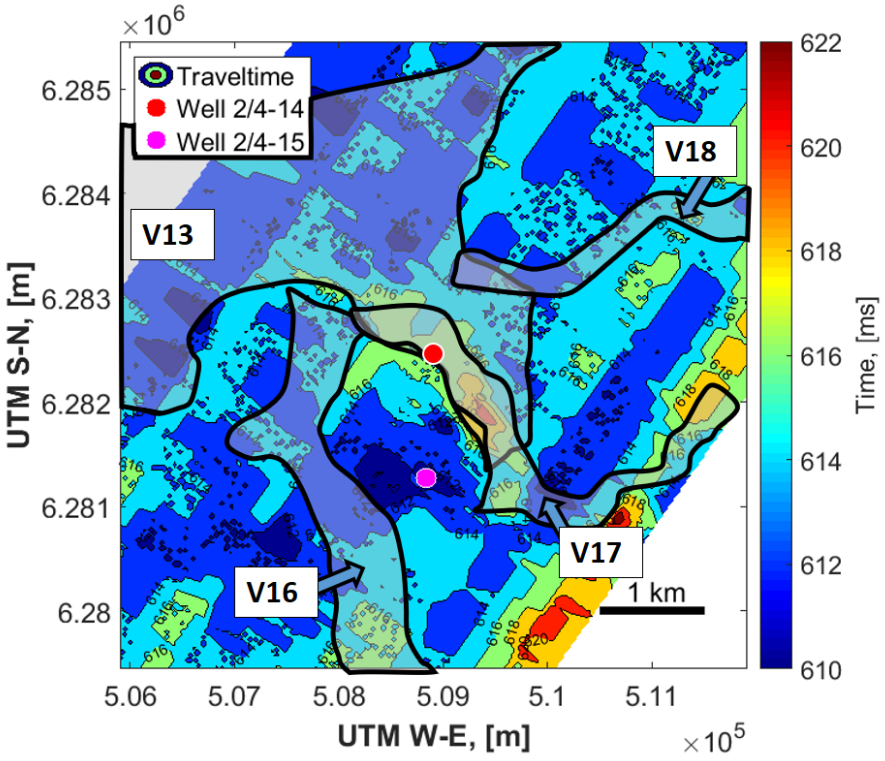

Figure 6.19: Traveltime to the first arriving refracted event at 1075 m offset. The bandpass filter used during the processing is (2-5-15-20) Hz. Tunnel valleys from Halvorsen (2012) are superimposed on top of the refraction traveltime contour plot.

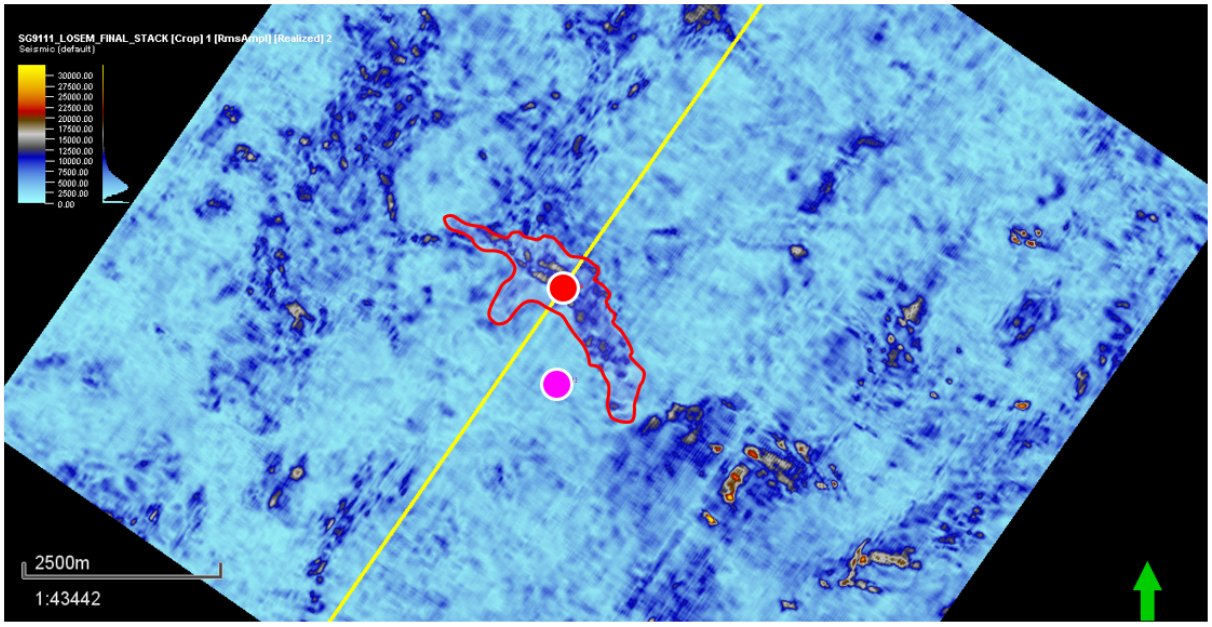

Figure 6.20: RMS amplitude at 224 ms for a 10 ms time-window. The red line around well 2/4-14 (red circle) is the interpreted extent of the anomaly seen in figure 6.16. The magenta circle marks the location of well 2/4-15 and the yellow line depicts the seismic section seen in figure 6.4.

Chapter 7

Discussion

There are some uncertainties regarding the results and they will be discussed in this chapter. Further some interpretations on from which depths the different refractions mapped at 3563 m offset are given. This is done by comparing the results from the refraction traveltime analysis with seismic sections, gamma-ray logs and the 3D cube. Note that the interpretations done here is one way of explaining the results, but there are probably other ways of interpreting the results as well.

7.1 Quality of seismic data

There were no issues with the raw data and the results of the processing were satisfying for both processing sequences. Initially, there was a concern that the different sail line directions would be visible in the results, but there were no clear indications of that.

The provided 3D cube was processed with the goal of imaging the shallow subsurface and proved to be useful for complementary analysis and to better understand the subsurface in the area with regards to the gas from the blowout.

7.2 Refraction analysis method

Assuming horizontal, homogeneous and isotropic layers the traveltime to a refracted event at a constant offset, is the same at any given position, in other words, if it was to be mapped it would appear flat (same traveltime everywhere). If then a gas anomaly is present in an area, the velocity in that area will be decreased, dependent on the saturation and properties of the gas.

Such anomaly would then straight up be visible when mapping the refraction traveltime, as the traveltime at the location of the gas anomaly would increase because of the decreased velocity. In reality, the subsurface is not horizontal and far from homogeneous and isotropic. In the study area, there are tunnel valleys that might influence the traveltimes and it was also shown that the subsurface is not horizontal in figure 6.5 where an interpretation of a seismic horizon is made.

To be able to compare traveltimes at different locations the offset is kept constant and assuming that the critical offset is constant, the distance travelled by the head-wave in the second layer also is constant which is crucial to be able to determine small traveltime differences. Because of that the subsurface neither is horizontal or homogeneous, the critical offset varies throughout the area.

To be able to have the best basis of finding these possible traveltime differences despite all the uncertainties some steps during processing of the data are taken. It is known that low frequencies give lower resolution in the seismic data, both vertically and horizontally. With this in mind, the frequency content in the data was lowered during the processing in ProMAX using an Ormsby bandpass filter.

Using the low-frequency filters the interfaces between layers appear flatter. When mapping the same refraction with the two different filters used in this thesis the difference is very clear. The higher frequency results show more than double the difference between the maximum and minimum traveltime and by just visually comparing the two, figure 6.2 and 6.16, the results using the lowest frequency data are clearly flatter.

In the seismic, the RMS amplitude of the hyperbolic reflection and linear refraction typically reaches it maximum in the right after the transition between the two, i.e. slightly higher than critical offset (Landrø et al., 2004). A decrease in velocity below an interface, keeping the velocity above constant, increases the critical offset. As the amplitude decrease, because of effects like geometrical spreading and absorption, the highest amplitudes along a refraction can be observed close to the critical offset. For most of the results presented in this thesis the largest refraction traveltimes correspond to the largest amplitudes, e.g. first arriving refraction at 1075 m seen in figure 6.2(traveltime) and 6.3(amplitude). This could indicate that the critical offset is increased for these large traveltimes, which also is consistent with a decrease in velocity for the layer below the refracting interface.

One can rewrite the equation for refraction traveltime for a two-layered model (equation

3.8) so it can be used for multiple layers. With this, it is in principle, possible to estimated layer thicknesses for multiple horizontal layers with increasing velocities. In reality, as the depth increase, this gets more and more difficult to identify individual layers. The deeper you go the bigger the chance is that the layers are not horizontal anymore and refractions from deeper layers often catch up to and arrive at receivers before the slower refractions from the shallower layers arrive. An upper practical upper limit to the method described is 3-4 layers (Landrø, 2010). For more complex cases, synthetic seismic modelling techniques are used, where you model the traveltime of the refracted waves, and change the geological model until the modelled traveltimes match the traveltimes observed in the seismic.

For the refraction at 1075 m offset it should be sufficient to assume a two-layered model and use the intercept in equation 3.8, which is what is done in this thesis. There are no good estimates of depths for the refractions mapped at 3563 m offset, some of the depths there are approximately found by comparing the results with the reflection data. In both cases, it would have been preferable to use synthetic seismic modelling to get better estimates of the depths, but there was not enough time to do this.

As in figure 3.1 the recorded refraction at a certain offset would have travelled along the refracting interface for a distance L. The observed apparent velocity would then be an average velocity along this subsurface line. The data is sorted and plotted as CDPs, meaning that the velocity average along the line L would be plotted in the middle. In other words, the anomaly could be observed by increased traveltimes at CDP locations outside of the anomaly. It is believed that this effect is very small and does not influence the results notably.

7.3 Refractions mapped at 3563 metre offset

The second processing sequence utilised a (2-5-15-20) Hz bandpass filter and an attempt of mapping the known gas anomaly at 490 m was made. After identifying refractions at a very high offset, figure 6.9, a simple method of plotting the trace at 3563 m offset for every CDP-gather was used. The resulting figure, figure 6.10, showed clear indications of increased traveltimes around the blowout well for almost all six refractions.

The brute stack shown in figure 4.3 and the refractions shown in figure 6.10 are from the same seismic line, SEQ051, which means the well location and CDP X-axis are the same for

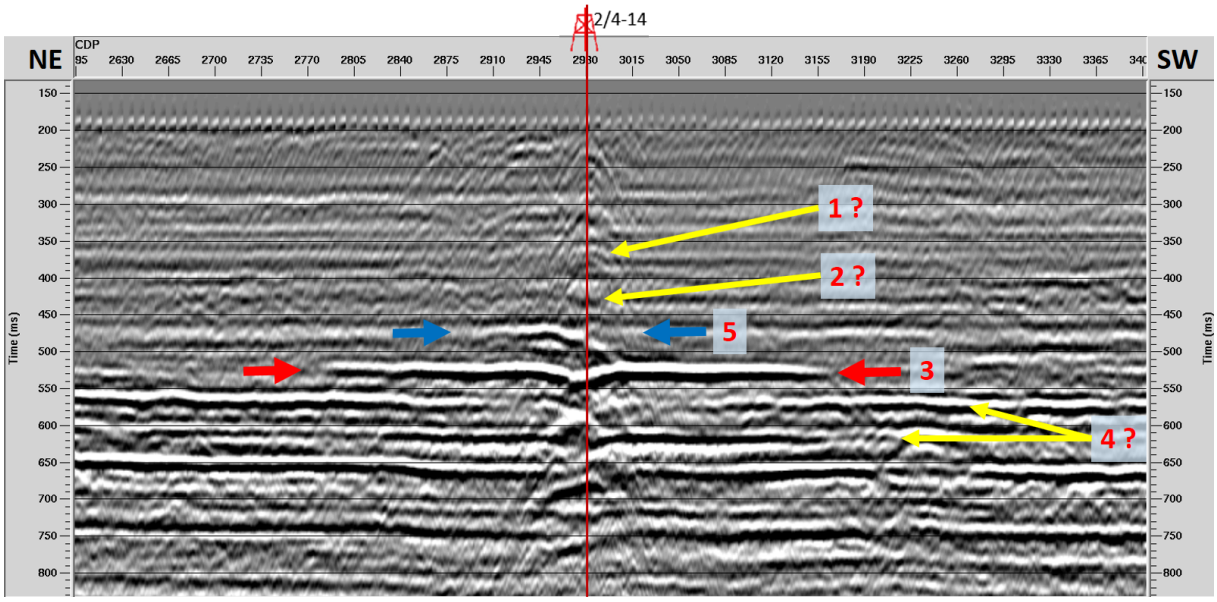

Figure 7.1: Zoomed in section of the brute stack from SEQ051, CDP range from 2595 to 3400 and correspond to a distance of approximately 5 km. The large gas anomaly seen at 520 ms around well 2/4-14 is marked with red arrows. Possible reflectors/depths associated with the five mapped refractions is marked with arrows. TWT axis goes from 150 to 800 ms. NE is to the left and SW is to the right.

both figures. Figure 7.1 shows a zoomed in section of the brute stack previously shown. The observed gas anomaly at 520 ms, marked with red arrows, stretch from approximately CDP 2780 to 3160, which is a distance of 2375 m. In the refraction traveltime data, the third refraction shows a notable increase in traveltime from approximately CDP 2783 to 3159, a distance of 2350 m.

In figure 2.1 the horizontal extent of the gas anomaly in the 3D cube can be seen. The gas appears to have migrated away from the well in all directions forming a more circular anomaly. For the mapped refraction traveltime in figure 6.13 the anomaly is elongated in the sail line direction (NE-SW). It can also be seen that for the anomaly the contour lines in the orthogonal direction of the sail line are more densely spaced than the ones in the sail line direction.

As mentioned in section 3.3 the amount of a 2D circular object with radius r observed along parallel lines, decrease rapidly as the distance from the centre of the object increase towards r. Similarly, a circular anomaly mapped with refraction traveltimes will show a similar effect towards the edge of the anomaly in the orthogonal direction of the shooting direction. In the shooting direction, the effect of the anomaly should increase linearly giving less dense spaced contour lines in the plot. So, a circular anomaly mapped with this refraction traveltime method would appear elongated in the sail line (shooting) direction.

Both the length of the anomaly and location of the anomaly in both data along SEQ051 match closely and at the same time the anomalies when seen from above correlate well with what is expected. With this, it is reasonable to believe that the refraction interface for this third event is at the base of the 520 ms gas anomaly reservoir, 500 m deep.

The fourth refraction mapped in figure 6.14 show very similar results as third refraction, but smaller in size and traveltime differences. The apparent average velocity is also higher, which generally indicate deeper layers. Since it is believed that the third refraction originates at 500 m and this refraction shows very similar traveltime trends one interpretation could be that the fourth refraction also is influenced by the gas in the 490-m sand, but is refracted at a deeper interface. It is also possible that this is a separate gas accumulation in one of the sand layers below the 490-m sand, e.g. at 523 m, 562 m or 602 m only with lower gas saturations causing the lower traveltime differences. Two possible candidates for reflections associated with this fourth refraction can be seen in figure 7.1.

Figure 6.15 shows the traveltime to the fifth refraction, of the refractions mapped this has the lowest apparent average velocity of 1790 m/s. In figure 6.10 the increased traveltime is observed from CDP 2879 to 3039 with higher traveltimes NE of the anomaly than SW. This extends only approximately 350 m in the SW direction of the well and 650 m NE of the well. This increase in traveltime might correspond to the reflection amplitude anomaly seen close to the well at 475 ms in the brute stack, marked with blue arrows in figure 7.1. This anomaly as well extends further NE of the well than SW but appears smaller in size going approximately from CDP 2890 to 3000, a distance of almost 700 m.

In this case, the anomaly around the well for the mapped refraction traveltimes appears circular in shape, following the same reasoning as earlier for the third refraction the shape of the anomaly, in reality, might be more elongated in the NW-SE direction. To investigate further the possible connection to the reflection anomaly at $\sim$475 ms in the brute stack an RMS amplitude timeslice at 476 ms in the 3D seismic cube is compared to the refraction anomaly.

Figure 7.2 show how the shape of the refraction traveltime anomaly of the fifth refraction compares to the RMS amplitude at 476 ms in the seismic 3D cube. It appears as there is a good correlation between the two. If one observes the highest refraction traveltimes for the refraction in figure 6.15 they are just east/northeast of the well which is the same location as where the highest RMS amplitudes are seen in figure 7.2 close to the well. Notice also how the RMS

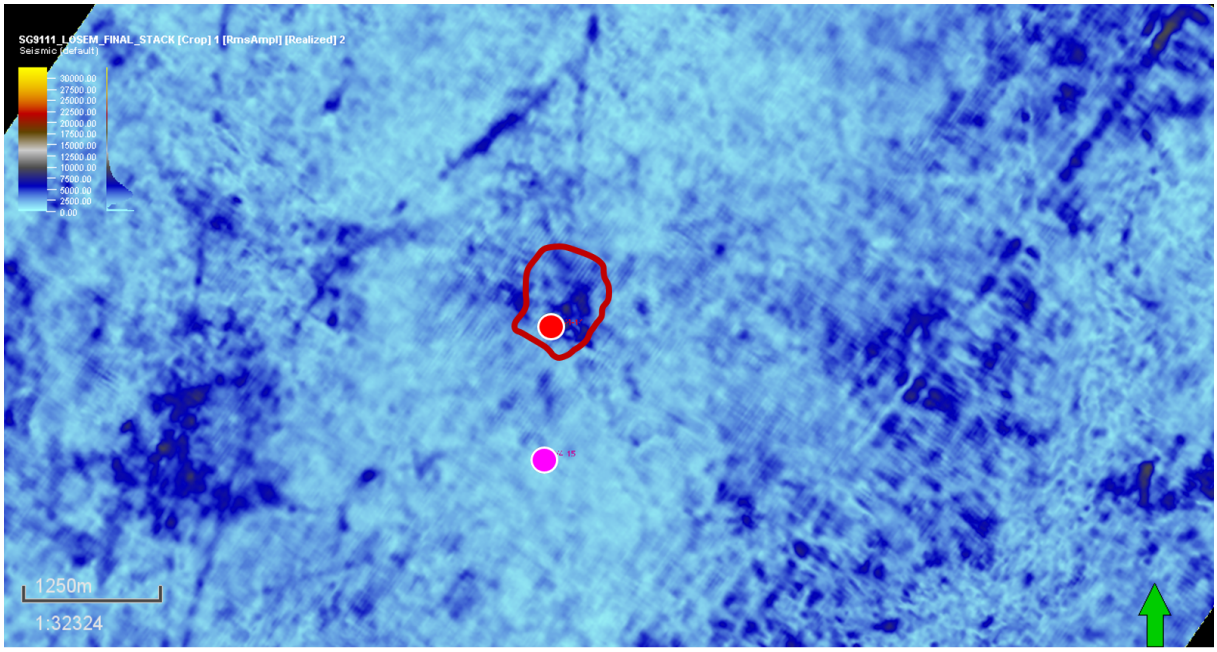

Figure 7.2: RMS amplitude at 476 ms for a 10 ms time-window in the 3D seismic cube. The red line that encircles the blowout well (red circle) is a conservative estimation of the anomaly seen for the fifth refraction in figure 6.15 interpreted approximately along the 2370 ms contour-line. Approximately 1.2 km south of 2/4-14 well 2/4-15 is marked with the magenta circle.

amplitude anomaly appears to be more elongated in the NW-SE direction. This is consistent with the previous statement on how the shape of a possible anomaly in the 3D cube would be.

With all these things in mind, it is reasonable to conclude that the fifth refraction is associated with the reflection at 475 ms in the reflection data.

The first two refractions are hard to say anything specific about other than that they arrive at this offset earlier with velocities not much lower than the third refraction. Because of this, it is believed that they originate at depths lower than 500 m. With the first arriving refraction having the shallowest refracting interface. Possible depths of these two refractions are shown in figure 7.1. The fact that there are no clear reflections that could correspond to these refractions does not mean that they image something that is not there. The low amplitudes could indicate that these refractions come from low reflection coefficient interfaces which are not visible in the reflection seismic. This illustrates the strength of this way of mapping the shallow gas using refraction seismic instead of reflection seismic.

7.4 Refraction at 1075 metre offset

The first refracted event at 1075 metre offset was mapped after both processing sequences with various success. It was evident that the lowest frequency bandpass filter illustrated best how the refractions can be used to map possible gas anomalies in these shallow layers.

7.4.1 First processing sequence

The first processing sequence utilised a (2-5-70-80) Hz bandpass filter. Throughout the area of interest, it became clear that being able to map this specific refraction everywhere was impossible. Refraction traveltimes after mapping this first refraction showed higher traveltimes close to the well than in the general area near the blowout well. Unfortunately, this was not consistent and high traveltime areas were visible at multiple locations. On closer inspection of the results is was evident that at the highest traveltimes the refracted event that originally was to be mapped was slowed down so much that it was caught up by another refraction. In addition to this, it appeared as the results suffered from the fact that the refracting interface was not horizontal.

It was of high interest to map the same refraction that Zadeh and Landrø (2011) used in their field data example as they used a similar method (only for 4D and timeshifts analysis) and found a refraction timeshift anomaly that they interpret as caused by gas from the blowout. By comparing shot gathers and estimates of depths and velocities from their paper with my results leads to the conclusion that the same refraction has been analysed. There are some differences off course, Zadeh and Landrø (2011) use 2D data from 1989 and 1990 with different acquisition parameters than for the 3D seismic data from 1991 used in this thesis. Despite this, the refraction is still the same and the results can be compared.

Since these relatively high-frequency data showed a result that was not as flat and clear cut as hoped an attempt to create a base refraction traveltime surface to estimate possible timeshifts was done. This attempt to estimate the refraction timeshift, figure 6.7,proved fairly successful. It appeared as the large traveltimes in the area SE of the wells became less pronounced which also was the case for the high traveltime areas west in the plot. Around the blowout well the increased traveltime seemed more consistent.

The comparison between estimated timeshift from the 1991 3D data and the refraction timeshift from 1988-1990 data was shown in figure 6.8. There were some similarities, espe-

cially SW of the blowout well where both results show negative timeshifts. NE of the blowout well there was a large difference between the two results. Further, as seen in the estimated timeshift map view in figure 6.7 there is no clear easily observed anomaly that can be interpreted as formed by blowout gas.

7.4.2 Second processing sequence

The second processing sequence utilised a (2-5-15-20) Hz bandpass filter. Mapping of the refracted event was successful and the same refraction was picked with confidence throughout the data. Figure 6.16 show the refraction traveltime and it can be seen that the traveltime differences throughout the area are much less than for the traveltime mapped after the first processing sequence. The effect of the lower frequency bandpass filter is clear and the result is now more like expected with the earlier assumptions such as horizontal layering.

Around the blowout well and SE of it, a traveltime anomaly was observed, the general traveltime is around 614 ms but around the well, it is above 616 ms. These higher traveltimes associated with the well are easily distinguishable from the rest of the area. There are high traveltimes in the SE, like the results from the first processing sequence, but these are believed to be caused by the increased depth to the interface in that area as seen in figure 6.5. As the higher traveltimes in the SE for the estimated refraction traveltime time-shift was much less pronounced than for the originally mapped refraction traveltime in figure 6.2, a similar effect on the second processing sequence results would be expected if a similar process to estimate the time-shift was applied.

The comparison between the refraction traveltime and time-shifts from Zadeh and Landrø (2011), shown in figure 6.17, showed a good correlation. Although the time-shift data show time-shifts further NE than the traveltime data it is believed that trend is caused by the same thing, shallow gas from the underground blowout. As the traveltime increase is consistent around the well it can be said figure 6.16 shows the horizontal extent of a shallow gas anomaly.

As seen in the resulting figure (figure 6.16) the survey line Zadeh and Landrø (2011) used goes straight through the highest traveltimes associated with the well. If they had picked some of the other surveys in the area they probably would not have found a time-shift as high as 4 ms.

7.4.3 Migration of the shallow gas

Tunnel valleys in the area was mapped in Halvorsen (2012) and compared with the refraction traveltime for the refraction mapped at 1075 m offset. It is possible that these tunnel valley acts as a conduit for gas migration from the blowout. As the depth of the different tunnel valleys were unknown and it is known that the different tunnel valleys can occur within each other the exercise of maybe finding some of them that could be used as migration paths for the gas seemed difficult.

As it turns out two of the tunnel valleys in the comparison showed a possible correlation with the gas anomaly and two showed little to no correlation, see figure 6.19. These two, V13 and V17, overlapped at the location of the anomaly but with further comparison with both the anomaly and the general traveltimes, it is believed that the gas has migrated into the tunnel valley V17.

Normally one would expect a circular anomaly around the well, like the gas accumulation at 490 m, seen in figure 2.1. For the refraction mapped at 1075 metre offset the gas anomaly is very elongated in the NW-SE direction with the highest traveltimes SE of the well. The fact that the gas might have migrated into V17 explains the lateral extent of this gas anomaly.

Observing the gas anomaly in figure 6.19 it is centred SE of the well which indicates that a large part of the gas has migrated away from the well, within the V17 tunnel valley. Landrø (2011) look at reflection time-shifts between 2009 and 1990 data for line 804 that goes through the blowout well in the SE-NW direction. In his figure (figure 14) there is an area approximately 2 km SE of the well that shows a relatively high time-shift. This area might be within V17 and if the gas already has migrated SE along this tunnel valley in 1991 there is a slight possibility that it could have migrated further and caused this time-shift that is observed between the 1990 and 2009 data. Important to note that this is circumstantial at best as the validity of the time-shift observed is uncertain and the migration of the gas is hard to predict. It would be interesting to find out if the tunnel valley V17 is this high permeability pathway for the gas and it has migrated this far from the well.

7.5 Validity of results

The refraction traveltime mapped in this thesis gives a ”static image” of the subsurface, and in reality the refraction traveltime anomalies could be caused by something else than gas from the underground blowout. For the refractions at 3563 m offset the anomalies are quite substantial, together with the fact that the appear around the blowout well leads to the conclusion that they are caused by gas from the blowout.

The traveltime anomaly found at 1075 m offset is not as clear as for the deeper refractions, and the horizontal extent is very unlike the others. With the comparison with refraction time-shift analysis this is also considered to be caused by the blowout gas.

The refraction traveltime results is in reality not comparable with the 4D refraction time-shift analysis in Zadeh and Landrø (2011). But in this case, the effect of the gas is so substantial that the mapped refraction traveltime illustrate the same effect as the 4D refraction time-shift and they can be compared.

Because of the way the refractions travel through the subsurface the apparent shape of the anomalies does not reflect the actual shape in the subsurface. Although the effect of this in 3D is somewhat unclear the anomalies are still there and cannot be dismissed.

Chapter 8

Overall summary, conclusion and recommendations for further work

8.1 Summary and conclusion

This thesis has investigated if a refraction seismic method can be used to map shallow gas, the method involved mapping the traveltime to refracted events.

Normally the offsets used for reflection seismic ranges from zero to 700 metres and for refraction seismic much higher offsets are utilised. The 3D data used for the refraction analysis in this thesis was not acquired for this purpose but had available offsets ranging from 175 to 3563 metres. The high offsets gave a high probability of refractions, from different interfaces, influenced by blowout gas to be recorded during acquisition.

The workflow set up to process and analyse the data proved to be time-consuming as each seismic line was processed separately and the analysis program had to be segmented because the hardware used was lacking the processing power to handle the analysis with this large amount of data. Despite these obstacles, the work-flow functioned as wanted.

The lateral extent of the possible gas anomaly found by Zadeh and Landrø (2011) was mapped with confidence. Comparing the refraction traveltime data with the time-shift data it was determined that the two methods imaged the same gas anomaly. A more circular anomaly centred around the blowout well was expected, but the shape of the anomaly was NW-SE directed with the biggest traveltimes 800 metres SE of the well. It was interpreted that the gas had migrated SE within a tunnel valley.

Gas anomalies at deeper interfaces were also mapped. Six refractions at 3563-metre offset were identified, five was attempted to be mapped and four was mapped successfully and showed traveltime anomalies around the blowout well. It is believed that the base of the sand layer at 490 metres and the associated gas was mapped. One possible interpretation of approximately which depths the different refractions originates was also presented.

The lack of time made the synthetic seismic modelling impossible, the estimated depths for the refractions at 3563-metre offset was based on general assumptions about the subsurface, experience with reflection and refraction seismic and comparison with reflection seismic.

The anomalies found in this thesis, that is believed to correspond to the anomalies in the reflection data, are much clearer and distinguishable from the surroundings in the refraction data. A good example of this was the fifth refraction interpreted to correspond to the 475 ms reflection where the RMS amplitude barely showed the anomaly whilst the refraction traveltime results were very clear. In addition, the second refraction shows a clear anomaly around the well but this cannot be found in the reflection data. This solidifies this method as a valuable complementary analysis for mapping shallow gas.

Traveltime analysis of refracted events proved to be a useful method of mapping velocity anomalies in shallow sedimentary layers. As the refractions are much more influenced by the velocity along the refraction interface than the reflections they can be used to locate possible velocity anomalies that cannot be found in the reflection seismic. There are many limitations to this method regarding the assumptions and the fact that there is a need of interfaces capable of creating refracted events. The interpretation of the refractions is complex, the depths to the different refractions is not easily found and the shape of a mapped anomaly does not necessarily reflect the actual shape of the anomaly in the subsurface. Some of the issues with the assumptions were overcome by specific processing steps.

In total five refractions were successfully mapped, where 2, possibly 4, of the anomalies observed might correspond to gas from the blowout that to this date is not mapped laterally. One refraction mapped at 1075 m offset showed a clear correlation with time-shift analysis done on the same refraction. From this, it was determined that this anomaly, from possible depths from 154 to 176 m, was caused by gas from the blowout. A link between tunnel valleys and the mapped gas was reasonable and it was interpreted that the gas has migrated (is migrating) within a tunnel valley. It was also observed that the major part of the gas at this depth, in the

three years from the blowout to the time of the seismic survey, had migrated approximately 800 metres SE.

Refraction traveltime analysis has proved valuable in evaluating shallow gas from the blowout. By applying this method in other areas one might be able to detect shallow gas/pressure anomalies that could be potential geohazards. With the increased interest to reduce risks in the industry, this could potentially give good complementary information about the shallow subsurface.

8.2 Recommendations for further work

A couple of days before the due date for this thesis a project report was brought to my attention. In this project refraction traveltime time-shifts were analysed along a different seismic line in the area, line 804, the same analysis like Zadeh and Landrø (2011) but along a different line. This line goes through the blowout well in the NW-SE direction. Due to the late attention to this analysis, it was not enough time to include it in this thesis. By visually comparing this analysis with my results it appears as there would be a very good correlation here as well, indicating that the understanding of the lateral extension of the gas anomaly is correct. This comparison should be included in further work.

In this thesis, there are uncertainties regarding the depths of the gas anomalies identified. Some were identified through comparison with reflection data, but the depths of other quite significant anomalies are still unknown. It is important to know where these gasses are, not only to be sure at where the gas from the blowout has migrated but also to get a better understanding of shallow subsurface hydrocarbon flow. Another aspect discussed in this thesis, and probably not fully understood, is the shape of the anomalies in the traveltime contour plots. Just a simple 3D seismic modelling scenario with differently shaped anomalies could give valuable insight to this. These things could be accomplished with synthetic seismic modelling or even better, full waveform inversion.

To get estimates of the volume of gas it is possible to establish a relation between gas saturation and refraction traveltime. A relation like this can be applied directly to the estimated time-shift or traveltime surface to find estimates of gas saturation.

This method has been tested for a blowout case, it would be interesting to see if it can be used in other cases. One interesting case would be looking at the CO_2 CCS (Carbon Capture

and Storage) project at Sleipner if the seismic acquired in that area includes high enough offsets for refractions influenced by the storage reservoir can be recorded.

To see the full potential of refraction seismic as a method of mapping the shallow subsurface a 4D quantitative analysis would be most interesting.

Bibliography

Arts, R., Chadwick, A., Eiken, O., Thibeau, S., Nooner, S., 2008. Ten years' experience of monitoring co2 injection in the utsira sand at sleipner, offshore norway. First Break 26, 65–72.

Breistøl, A. H., 2015. Broadband processing of conventional 3d seismic data for near surface geohazard investigation: A north sea case study. Master's thesis, Norwegian University of Science and Technology.

Chadwick, R. A., Zweigel, P., Gregersen, U., Kirby, G., Holloway, S., Johannessen, P., 2004. Geological reservoir characterization of a co2 storage site: The utsira sand, sleipner, northern north sea. Energy 29, 1371–1381.

Cofaigh, C. O., mar 1996. Tunnel valley genesis. Progress in Physical Geography 20 (1), 1–19. URL https://doi.org/10.1177%2F030913339602000101

Halvorsen, H. S., 2012. Mapping of shallow tunnel valleys combining 2d and 3d seismic data. Master's thesis, Norwegian University of Science and Technology.

Hansteen, F., Wills, P. B., Hornman, K., Jin, L., Bourne, S., jan 2010. Time-lapse refraction seismic monitoring. In: SEG Technical Program Expanded Abstracts 2010. Society of Exploration Geophysicists, pp. 4170–4174.
URL https://doi.org/10.1190%2F1.3513735

Landrø, M., 2010. Anvendt geofysikk. Compendium used as lecture notes in course Applied Geophysics at NTNU.

Landrø, M., jun 2011. Seismic monitoring of an old underground blowout - 20 years later. First Break 29, 39–48.
URL https://doi.org/10.3997%2F1365-2397.2011017

Landrø, M., Nguyen, A. K., Mehdizadeh, H., jan 2004. Time lapse refraction seismic - a tool for monitoring carbonate fields? In: SEG Technical Program Expanded Abstracts 2004. Society of Exploration Geophysicists.
URL https://doi.org/10.1190/1.1845218

LOSEM, 2016. Losem processing. Powerpoint presentation about processing of a 3D seimsic dataset, powerpoint created by Jamshade Khan.

MathWorks, 2016. The language of technical computing. Website, last accesed date: 28.10.2016.
URL https://se.mathworks.com/products/matlab/

NORLEX, n.d. Nordland group. website, last accessed: 04.05.2017.
URL http://nhm2.uio.no/norges/litho/nordland.php

NPD, N. P. D., n.d. Well 2/4-14. Website, last accessed: 15.05.2017.
URL http://factpages.npd.no/FactPages/Default.aspx?nav1=wellbore&nav2=PageView|Exploration|All&nav3=1343&culture=en

Schlumberger, 2017a. Oilfield glossary, diffractions definition. Website, last accessed: 08.06.2017.
URL http://www.glossary.oilfield.slb.com/Terms/u/underground_blowout.aspx

Schlumberger, 2017b. Oilfield glossary, underground blowout definition. Website, last accessed: 15.05.2017.
URL http://www.glossary.oilfield.slb.com/Terms/u/underground_blowout.aspx

Schlumberger, 2017c. Petrel e&p software platform. Website, last accessed: 12.06.2017.
URL https://www.software.slb.com/products/petrel

Sheriff, R. E., Geldart, L. P., 008 1995. Exploration Seismology:, 2nd Edition. Cambridge University Press, Cambridge.

Zadeh, H. M., Landrø, M., jan 2011. Monitoring a shallow subsurface gas flow by time-lapse refraction analysis. GEOPHYSICS 76 (6), O35–O43.
URL https://doi.org/10.1190%2Fgeo2011-0012.1

Appendix A

Variable density plot

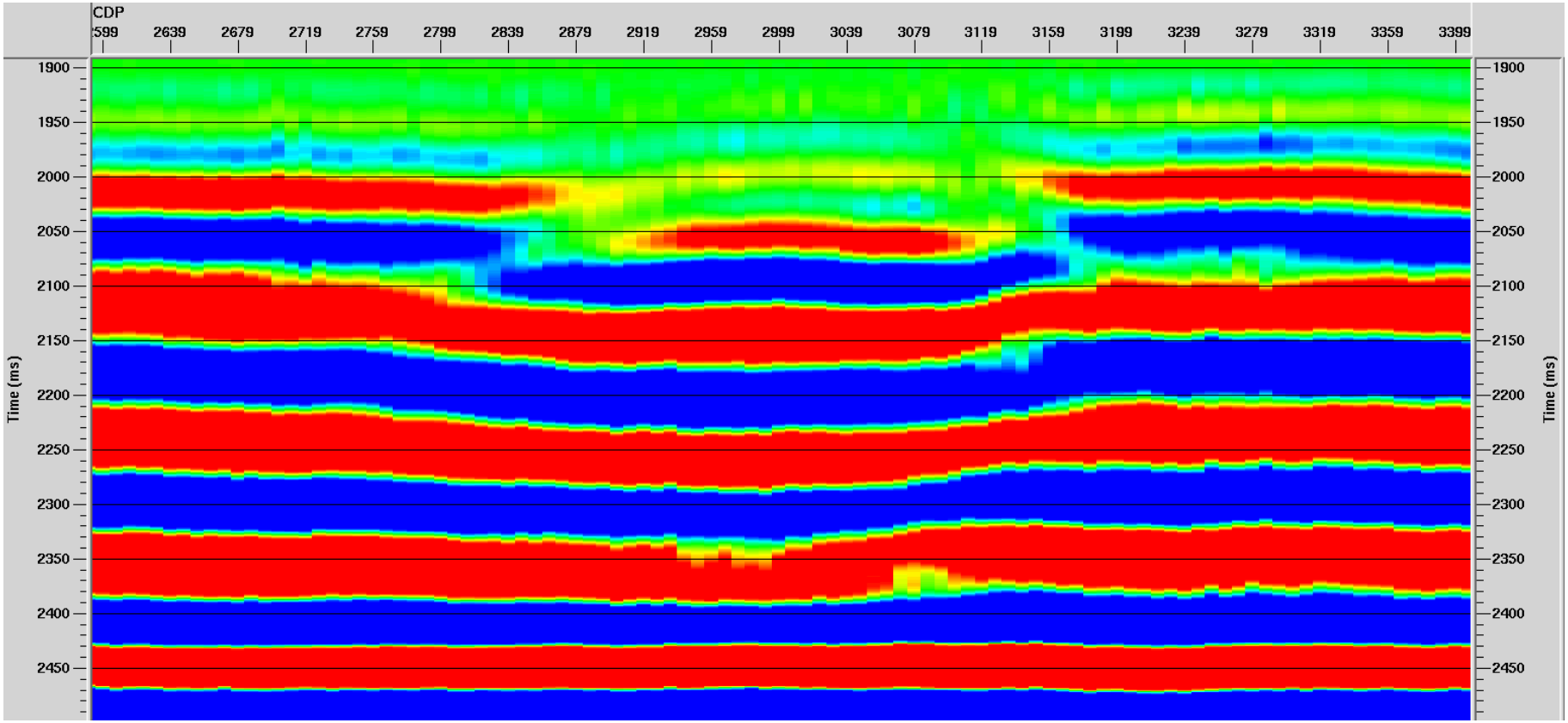

Figure A.1: Variable density trace at offset 3563 m for each common depth point along line SEQ051 that crosses well 2/4-14. The well is situated at approximately CDP 2950 in the middle of the figure, the distance from left to right is 5 kilometres. The traces are gained up significantly to be able to see the refraction at 1950 milliseconds. The sail direction is SW, hence SW is to the right and NE is to the left.

Appendix B

Additional figures from results

In this appendix additional figures from the results in chapter 6 are shown.

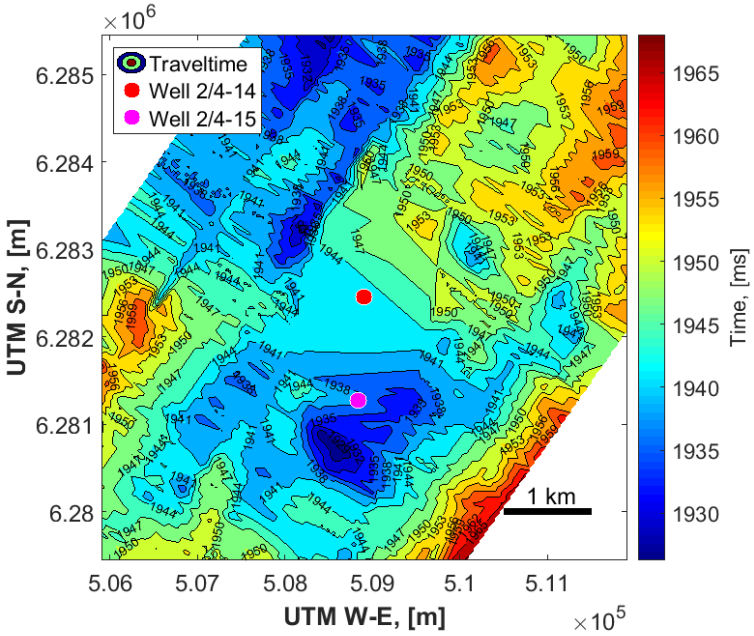

Figure B.1: Traveltime to the first arriving refracted event at 3563 m offset. The bandpass filter used during the processing is (2-5-15-20) Hz. X and Y-axis are in UTM coordinates and wells 2/4-14 and 2/4-15 are marked.

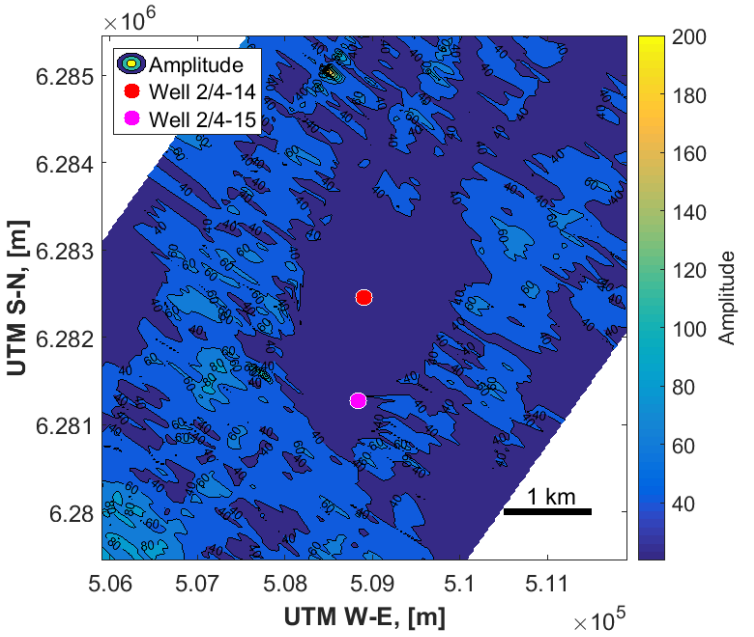

Figure B.2: Amplitude contour plot of the first arriving refracted event at 3563 m offset. The bandpass filter used during the processing is (2-5-15-20) Hz. Amplitudes here correspond to the traveltime contour plot shown in figure B.1. X and Y-axis are in UTM coordinates and wells 2/4-14 and 2/4-15 are marked.

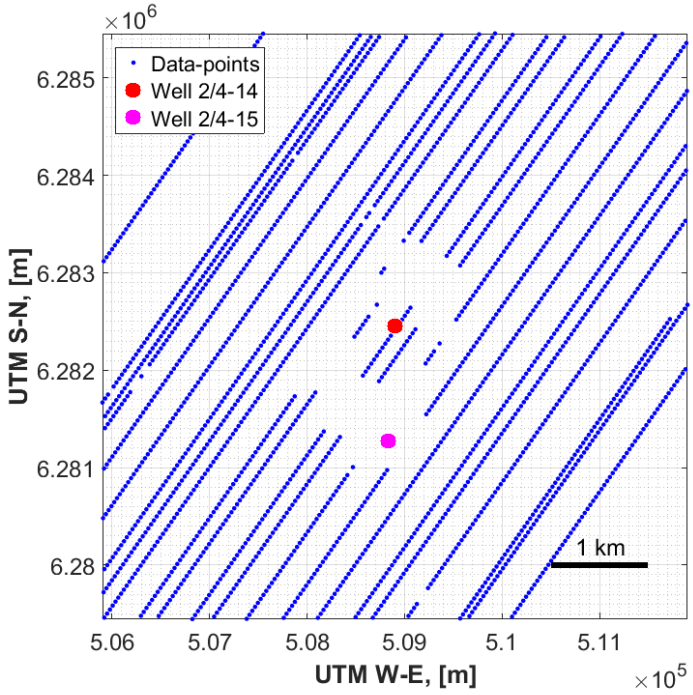

Figure B.3: Data-points used to generate traveltime contour plot for the second arriving refracted event at 3563 m offset shown in figure 6.12. The bandpass filter used during the processing is (2-5-15-20) Hz. The picked data-points that are excluded from further analysis are shown as red asterisks.

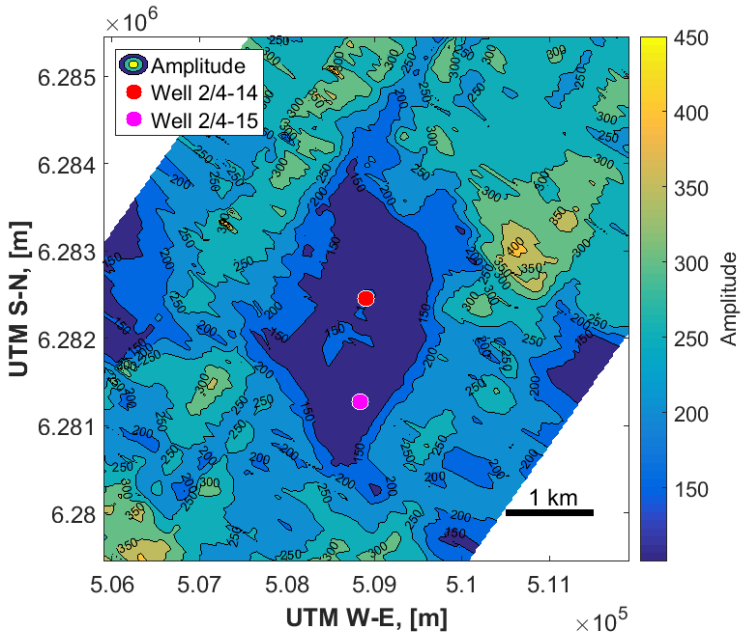

Figure B.4: Amplitude contour plot of the second arriving refracted event at 3563 m offset. The bandpass filter used during the processing is (2-5-15-20) Hz. Amplitudes here correspond to the traveltime contour plot shown in figure 6.12. X and Y-axis are in UTM coordinates and wells 2/4-14 and 2/4-15 are marked.

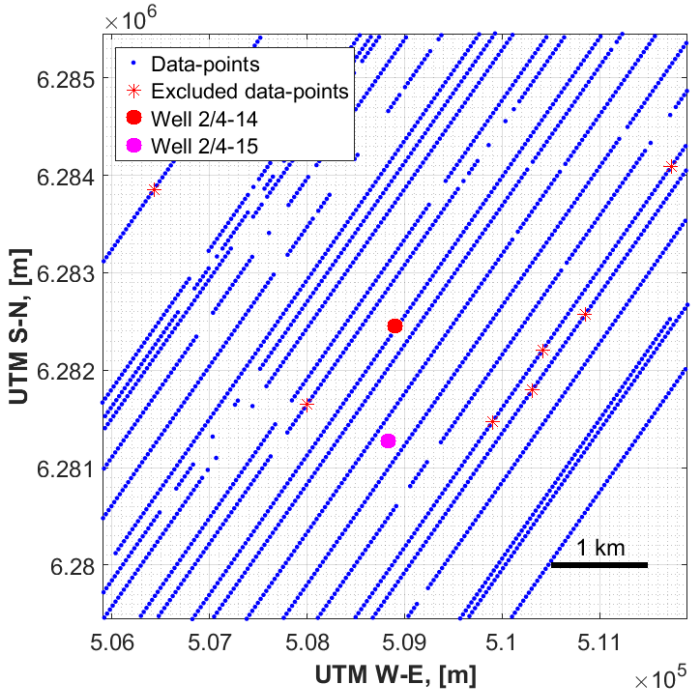

Figure B.5: Data-points used to generate traveltime contour plot for the third arriving refracted event at 3563 m offset shown in figure 6.13. The bandpass filter used during the processing is (2-5-15-20) Hz. The picked data-points that are excluded from further analysis are shown as red asterisks.

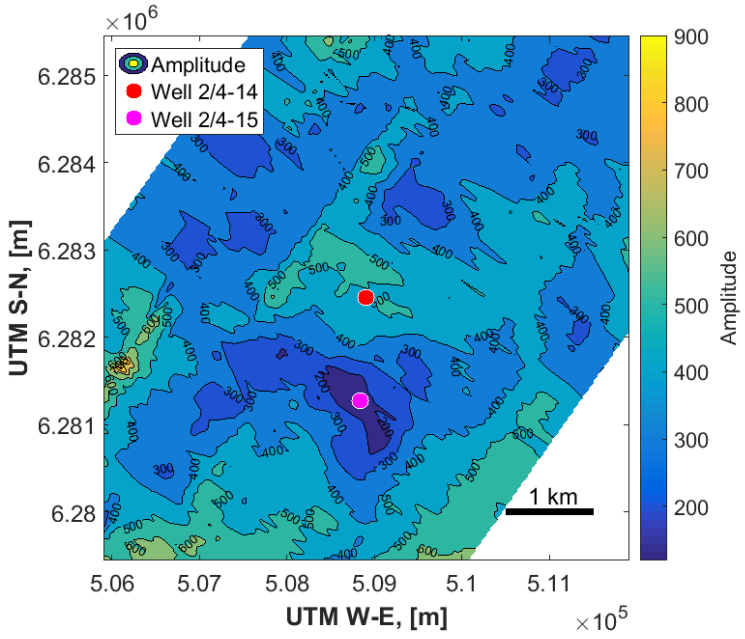

Figure B.6: Amplitude contour plot of the third arriving refracted event at 3563 m offset. The bandpass filter used during the processing is (2-5-15-20) Hz. Amplitudes here correspond to the traveltime contour plot shown in figure 6.13. X and Y-axis are in UTM coordinates and wells 2/4-14 and 2/4-15 are marked.

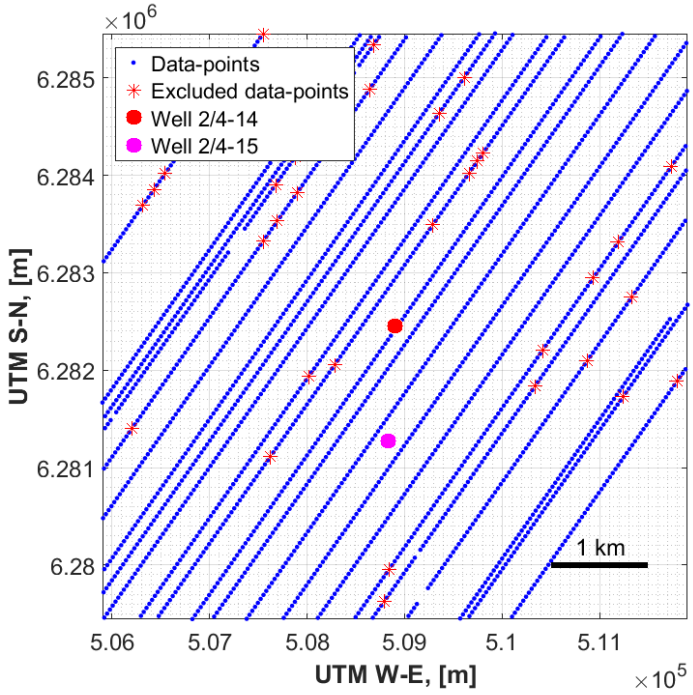

Figure B.7: Data-points used to generate traveltime contour plot for the fourth arriving refracted event at 3563 m offset shown in figure 6.14. The bandpass filter used during the processing is (2-5-15-20) Hz. The picked data-points that are excluded from further analysis are shown as red asterisks.

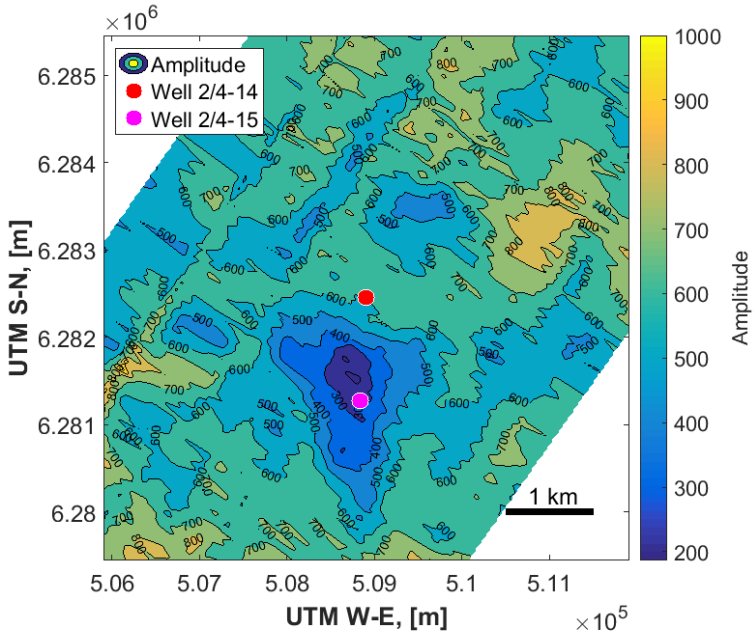

Figure B.8: Amplitude contour plot of the fourth arriving refracted event at 3563 m offset. The bandpass filter used during the processing is (2-5-15-20) Hz. Amplitudes here correspond to the traveltime contour plot shown in figure 6.14. X and Y-axis are in UTM coordinates and wells 2/4-14 and 2/4-15 are marked.

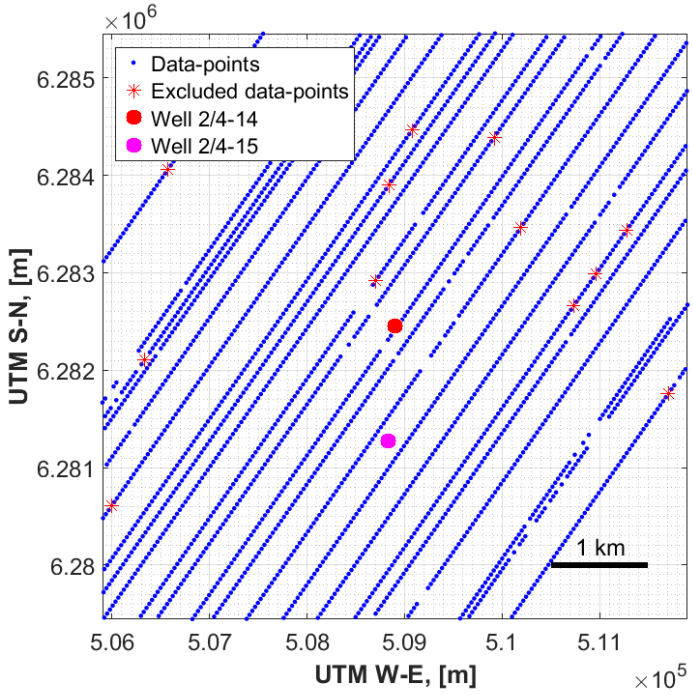

Figure B.9: Data-points used to generate traveltime contour plot for the fifth arriving refracted event at 3563 m offset shown in figure 6.15. The bandpass filter used during the processing is (2-5-15-20) Hz. The picked data-points that are excluded from further analysis are shown as red asterisks.

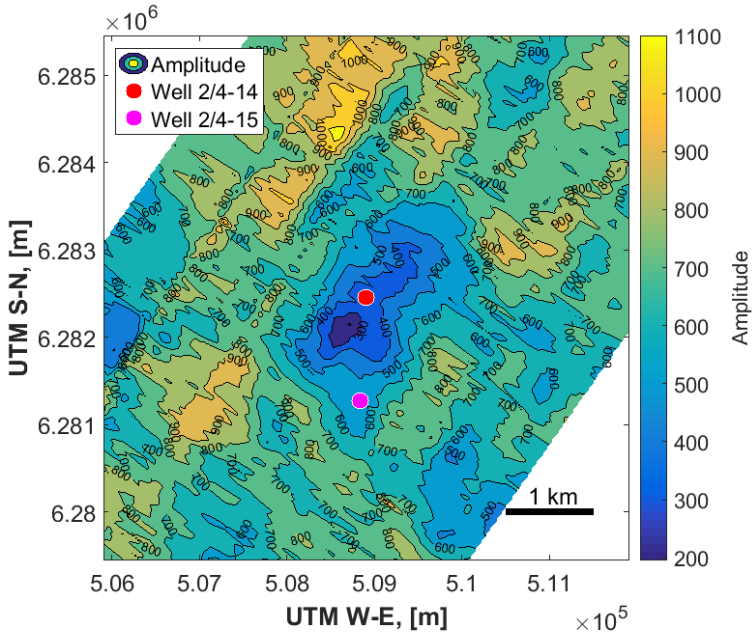

Figure B.10: Amplitude contour plot of the fifth arriving refracted event at 3563 m offset. The bandpass filter used during the processing is (2-5-15-20) Hz. Amplitudes here correspond to the traveltime contour plot shown in figure 6.15. X and Y-axis are in UTM coordinates and wells 2/4-14 and 2/4-15 are marked.

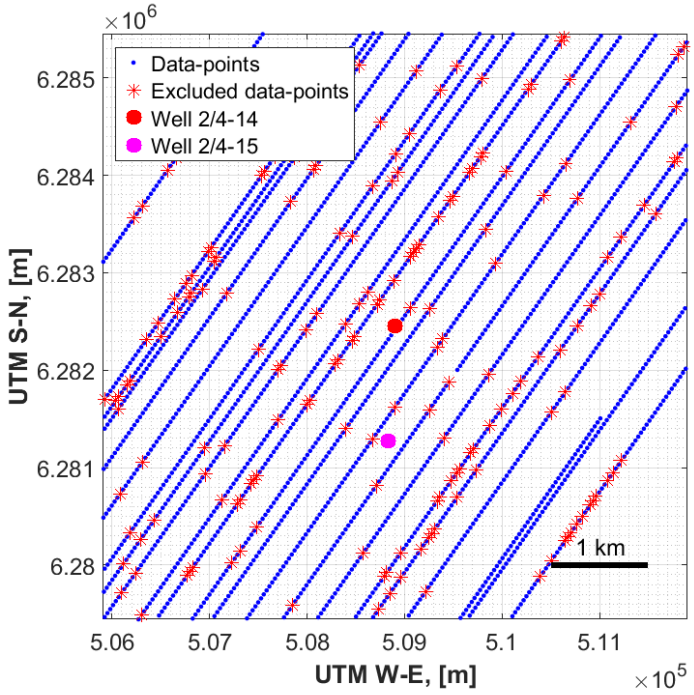

Figure B.11: Data-points used to generate results shown in figure 6.16. The bandpass filter used during the processing is (2-5-15-20) Hz. The picked data-points that are excluded from further analysis are shown as red asterisks.

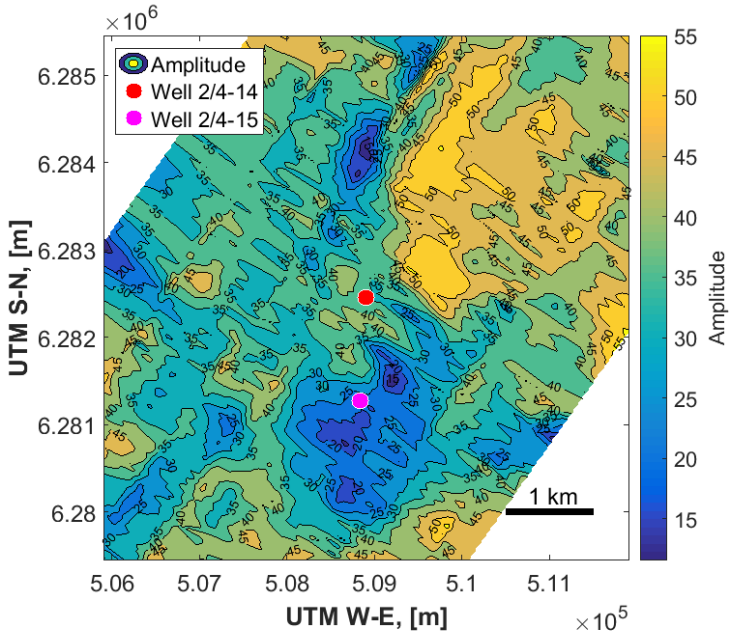

Figure B.12: Amplitude contour plot of the first arriving refracted event at 1075 m offset. The bandpass filter used during the processing is (2-5-15-20) Hz. Amplitudes here correspond to the traveltime contour plot shown in figure 6.16. X and Y-axis are in UTM coordinates and wells 2/4-14 and 2/4-15 are marked.

Appendix C

Zadeh and Landrø (2011) time-shift result

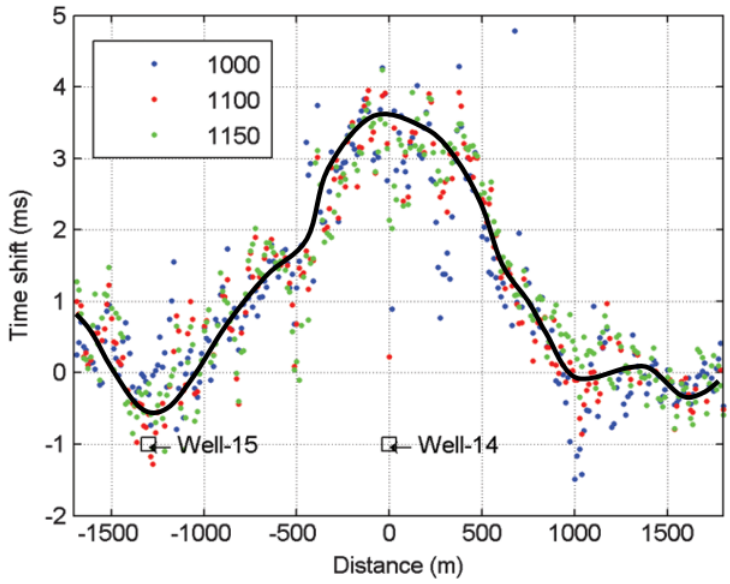

Figure C.1: Cross-correlation time-shift for offsets ranging from 1000 to 1150 m. A 50-ms timewindow is used to calculate the cross-correlation. Well locations are shown with boxes. A time-shift of 4 ms is observed around the blowout well-14. Horizontal axis shows the distance from the blowout well in metres. Figure and caption is taken from Zadeh and Landrø (2011), the black curve show the manual interpolation used to compare with results from this thesis.

Appendix D

Tunnel valleys

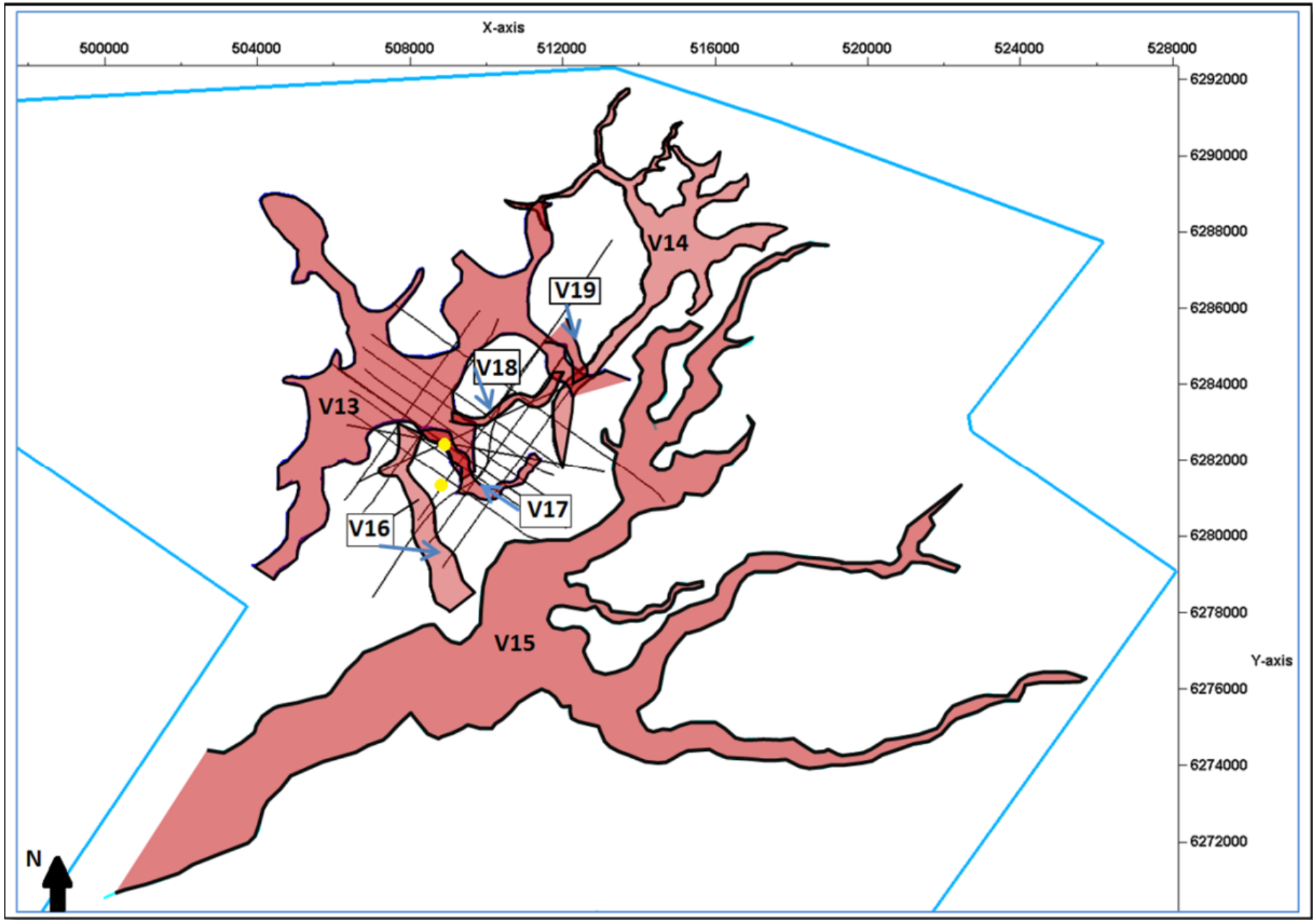

Figure D.1: Overview map of the seven tunnel valleys mapped below first seabed multiple (¿180ms TWT). The clear blue line marks the boundary of the seismic 3D cube and black lines 2D surveys in the area. The yellow dots marks well 2/4-14 and 2/4-15. The tunnel valleys have a dominating (SW-NE) direction. The figure is taken from Halvorsen (2012).